Dry Metal Forming Open Access Journal

Final Project Report

Edited by Frank Vollertsen
Available online at https://elib.suub.uni-bremen.de

www.drymetalforming.de

Dry Met. Forming OAJ FPR 6 (2020) 192–227
Date of Report 31 May 2020; published 12 June 2020

Potentials of Dry Rotary Swaging

(DFG Grant No. KU 1389/14; RI 1108/5; ZO 140/13, Funding Period 01.01.2014 – 30.06.2020)

Henning Hasselbruch[1*], Marius Herrmann[2,3,4], Julian Heidhoff[1,4], Florian Böhmermann, Oltmann Riemer[1], Andreas Mehner[1] and Bernd Kuhfuss[2,3,4,]

[1]IWT, Leibniz Institute for Materials Engineering, Badgasteiner Str. 3, Bremen, 28359 Germany
[2]bime, Bremen Institute for Mechanical Engineering, Badgasteiner Str. 1, Bremen, 28359 Germany
[3]MAPEX Center for Materials and Processing, Germany
[4]University of Bremen, Bremen, Germany

Summary

Infeed rotary swaging is an appropriate cold massive forging technology for the manufacture of cylindrical shaped components made of iron or aluminum base alloys. The process is focused on reducing the cross-section of full profiles or tubes and is e.g. widely used in automotive industry. The design of swaged hollow components can easily be adapted to the external load in such a way, that the wall thickness is partially reduced and the material cross-section is increased where needed. The above-mentioned advantages result in a high potential for light-weight production while the produced components exhibit high geometric accuracy and surface quality. However, an excellent CO_2 balance is yet limited due to high demands for lubricants significantly increasing the number of process steps for further component refinement.

In order to increase the overall process efficiency, a changeover to a dry process design becomes necessary. A dry processing will cause high die wear and deterioration of workpiece quality. The most important functions of the lubricant have to be substituted by other approaches and strategies. Development and removal of heat, generation and discharge of wear debris and, above all, die wear and the resulting workpiece quality have to be considered. The effective tribological friction conditions have to be adjusted by means of geometric adaptations of the active die surfaces to realize good workpiece qualities at comparable cycle times.

This paper gives a review of the state-of-the-art in dry rotary swaging. Extensive experiments in laboratory scale as well as application tests were performed with various die setups. The most important findings regarding wear, wear minimization, process kinematics, workpiece quality, FEM simulation are presented. The overarching goal is to achieve a long-term stability for the successful dry processing.

Keywords: Infeed rotary swaging; dry cold massive forming; PVD-a-C:H coatings; structured dies, FEM

Nomenclature

A	amplitude (mm)
a_e	radial depth of cut (µm)
d_0	initial diameter of the part (mm)
d_1	final diameter of the part (mm)
d_c	cylinders initial diameter (mm)
F_A	axial reaction force (N)
F_f	feed force (N)
F_{Norm}	normalized force (-)
F_R	radial force (N)
F_{st}	stroke frequency (Hz)
f_z	feed per tooth (µm)

*E-mail address of corresponding author: hasselbruch@iwt-bremen.de

H	height of the tip of the part (mm)
h_c	cylinders initial diameter (mm)
h_d	drop height (m)
h_T	die stroke (mm)
L_0	initial length of the tensile specimens (mm)
L_{cal}	length of the die calibration zone (mm)
l_{cal}	length of calibration zone (mm)
l_{die}	die length (mm)
l_{st}	feed per stroke (mm/stroke)
v_f	feed rate (mm/min)
r_0	initial work piece radius (mm)
r_1	final work piece radius (mm)
r_{nom}	nominal radius by the closed dies (mm)
RONt	roundness deviation (µm)
S	structure value (µm)
s_0	wall thickness (mm)
s	empirical standard deviation (mm)
S_a	surface roughness (µm)
z	infeed length (mm)
α	die angle (°)
α_{eff}	effective die angle (°)
λ	wavelength (mm)
μ	friction (-)
μ_{Red}	friction coefficient in the reduction zone (-)
μ_{Cal}	friction coefficient in the calibration zone (-)
Δx	back motion (mm)
I	reduction zone
II	calibration zone
III	exit zone
AlTiCN	aluminum titan carbonitride
a-C:H	hydrogen-containing amorphous carbon
CO_2	carbon dioxide
CrN	chromium nitride
DLC	diamond like carbon
FEM	Finite Element Method
NP	neutral plane
PVD	physical vapor deposition
Si	silicon
TiAlN	titanium aluminum nitride
TiC	titanium carbide
TiN	titanium nitride
W	tungsten
WC-Co	tungsten carbide cobalt layer

1 Introduction

Rotary swaging belongs to the sustainable and resource-efficient production techniques and is especially used in the automotive industry [1] for the manufacture of components such as gear shafts, axle shafts, compensating shafts or steering spindles primary made of tubular semi-finished products [2]. Rotary swaging is an incremental forging process offering a high potential for light weight parts [3].

This production process is characterized by a number of advantages including an undisturbed fiber flow which is leading to an optimized utilization of the workpiece material. Strain hardening, adjustable by the ratio of deformation, increases the static and dynamic component application strength [4]. As a result, a sufficient dimensional accuracy [5] as well as surface quality [6] can be achieved during forming. Due to the use of

mandrels also complex internal geometries, e. g. internal profiling, are producible [7]. Furthermore, components with locally adapted wall thicknesses are realizable with by a flexible process adjustment at short cycle times increasing the overall efficiency [8].

A drawback for the environmental balance of conventional infeed rotary swaging is the need for large quantities of lubricant which are usually based on mineral oils with native and derivative lipid substances also containing sulfur additives. In order to achieve process reliability and sufficient workpiece qualities, the lubricants have to assume important functions: lubrication of the complete swaging unit, guiding surfaces and active surfaces in the forming zone, separation of workpiece and die surfaces, cooling of the whole process zone and forming unit and the active discharge of wear debris. A considerable amount of lubricant is lost due to sticking to the workpiece surfaces. On the other hand, the remaining lubricants have to be separated from wear debris by expensive re-cycling steps.

A dry process design and thus the renouncing of lubricants are of considerable interest to machine manufacturers and operating personal. On the one hand, more favorable tooling materials could be used and on the other hand, the potential health burden of the staff would be reduced [9]. In particular, the produced components could be directly subjected to further finishing operations without the need of complex purification steps. However, the lubricant functions have to be substituted by novel strategies, since a dry process design is directly associated with increased die wear and insufficient workpiece quality. Depending on the workpiece material dry forming can even lead to an unstable process. In the following chapters the conventional infeed rotary swaging and novel, interdisciplinary approaches will be presented. Fundamental experiments in laboratory scale as well as various application tests were conducted. Strategies for future developments will be presented as well.

1.1 Conventional infeed rotary swaging

Rotary swaging has been used in production industry for more than 100 years. First scientific research approaches go back to the 1960s [10]. In the recent past, numerous works have to be mentioned related to their fundamental character with focus on infeed rotary swaging [11], plunge rotary swaging [12], process simulation [13], production route [14]. Fig. 1a illustrates an opened serial swaging unit. In general, three or four dies are concentrically arranged around the workpiece. As soon as the unit starts rotating, the cylinder rollers run over the base jaws which are equipped with a small sinusoidal cam at the head leading to a die stroke movement h_T, see Fig. 1b. Due to a constant rotational speed of the swaging unit during forming, centrifugal forces cause a reopening of the dies. Then the workpiece is axially fed in the center of the swaging unit by a linear direct drive. The incremental forging with a constant frequency is initiated from the first contact in the calibration zone, zone I. The required feed force F_f is also depending on the die angle α [15]. Typical die angles are between 5 ° and 15 °. It can be excluded that the processes are running under self-locking at lower die angles.

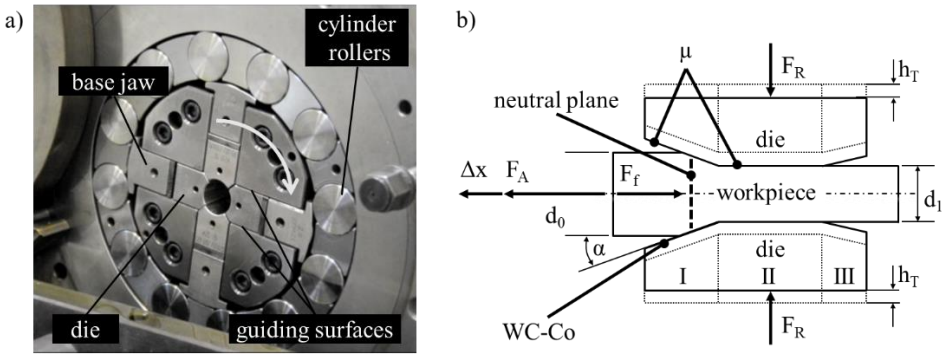

Fig. 1: Infeed rotary swaging process: a) Open swaging unit and b) process kinematics

The forming primarily takes place in radial direction, represented by F_R. Depending on the frictional conditions μ which are dominating in the reduction zone, the resulting axial reaction force F_A is counteracting the feed force F_f which is limited by the workpiece material strength. When the coefficient of friction is increased in zone I the reaction force F_A decreases. This is conventionally realized by a rough thermally sprayed tungsten carbide cobalt layer (WC-Co) in zone I. The axial reaction force F_A can cause a backwards motion of the feeding systems Δx. In this context, the position of the neutral plane in axial direction is also affected by friction. At the neutral plane the workpiece material flow is reversed in its axial direction and flows only radial

[16]. As a desired result of increased friction, the neutral plane shifts in the direction of the preform corresponding with an increased material flow in feed direction at each die stroke [17].

First dry processing is mentioned in the work of Groche et al. and is focused on the process kinematics when cold forming of 16MnCr5 [18]. It could be determined at a constant die angle α of 5° that the axial reaction force drastically decreases by the use of roughened die surfaces (WC-Co) under lubrication or by the use of smooth surfaces in a dry forming process. Dörr et al. investigated alternative lubricant concepts on aqueous basis [19]. The aim of their work was to reduce the consumption of mineral oil. The forming temperatures were measured by a Pt100 thermocouple integrated in the die close to the active forming zones. It was found that the cooling effect is significantly improved compared to the lubricants based on mineral oil. Furthermore, hot rotary swaging without lubricant of steel above the recrystallization temperature (800 °C) for a material improvement of structural steel S355J2C was investigated [20].

1.2 Approach

The lack of lubricant in a dry rotary swaging leads to a missing separation between die and the newly created workpiece surfaces due to the forming operation and causes increased material adhesions on the die surfaces which results in a deterioration of the workpiece quality. The die angle, feed rate and material strength of the workpiece, high pressures per unit area as well as increased shear stresses lead to abrasive die wear and instable swaging processes. In order to encounter these challenges three approaches were pursued: modeling and simulation, the application of defined surface structures and the deposition of thin hard coatings, as shown in Fig. 2. The aim of these approaches is to achieve a similar process robustness and workpiece quality compared to conventional lubricated rotary swaging.

In a first step, the process is modeled and simulated to investigate the effect of die structuring in the reduction zone. An appropriate macrostructure in the reduction zone allows to modify and control the axial reaction force. And an appropriate micro-structure in the calibration zone is applied in order to reduce the local adhesive wear in the calibration zone. Furthermore, an active particle discharge has to be facilitated by the geometrical design of the surface structures. The entire forming zone has to be protected against adhesive and abrasive die wear. In particular, the applied structures must be protected against deformation and clogging by application of hard and low friction coatings with a minimum tendency of adhesive wear against steel and aluminum alloys. An increased workpiece quality, e. g. the surface roughness or the geometrical accuracy, is also achieved by a low tendency of cold welding. A low coefficient of friction is useful to support the removal of wear debris out of the forming zone. Coatings with sufficient fracture toughness and adhesion to the steel substrate are required due to the highly dynamic loads during the rotary swaging process. A combination of structuring and coating will be used for an effective functionalization of the surface of rotary swaging dies for dry processing.

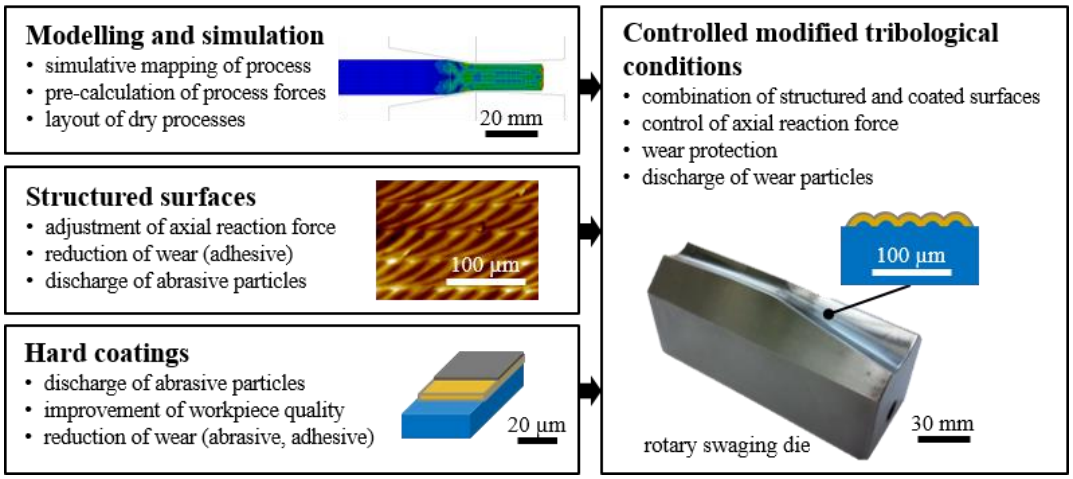

Fig. 2: Interdisciplinary approaches for a successful dry process design, cf. [21]

1.2.1 FEM

The rotary swaging process is investigated by experiments and by modeling and simulation. One approach is the "upper bound method" [16], which allows a prediction of process forces [22] and the flow of material in the workpiece [23]. The "slab method" or body equilibrium method is also used, for the investigation of different die geometries with [24] or without the usage of a mandrel [25]. A further method is the "Finite Element

Method" (FEM), whereby the influence of different die geometries is examined by means of three-dimensional modeling [26]. The comparison of the "slab method" and FEM shows a good agreement and both methods are suitable for rotary swaging [27]. A disadvantage of 3D-FEM, however, is the high computing time, which can be reduced by simplification to a 2D-axial-symmetric simulation [28]. For the investigation of influences such as infeed per stroke, die or workpiece geometry on the process, a 2D axisymmetric simulation is well suited compared to a 3D simulation [15]. Thus, the material flow [17], forming forces [29] or material strains [30] are also meaningfully simulated in 2D axial symmetric simulations.

1.2.2 Structuring of the forming dies

The surface topography essentially affects the friction and wear properties of the forming die. Macro- and micro-structured forming die surfaces have the potential to contribute to the development of dry forming processes. The tribological properties of the die surfaces are directly related to their micro- and macro topography. Macrostructures with dimensions of several millimeters change the geometrical contact conditions between the die and the workpiece, as proposed by Brosius et al. for deep drawing [31]. Dies and blank holders with macrostructures arranged concentrically around the drawing gap reduce the contact area between die and blank holder to the sheet by up to 80 %. As a result, the blank holder force could be reduced by 90 %. In contrast to deep drawing with conventional and unstructured dies, the occurring contact pressure at the contact surfaces between die and workpiece is substantially reduced and allows for a dry process control [31]. Microscopic structures, which can be characterized by parameters of the roughness measurement technique, change the interaction of the die and the workpiece at the microscopic level and contribute to a reduction of the dry friction. This concept has been successfully tested for dry micro-sheet forming by Böhmermann et al. [32]. This concept was realized by micro-milling of the final die surface using optimized milling variables such as feed per tooth f_z or radial depth of cut a_e [33]. Moreover, these microstructures also prevented the movement of wear debris along the forming zone avoiding an increase of the effective friction and die wear by surface ploughing in dry contact [34]. Even if the tribological effectiveness of structured die surfaces has already been proven in literature, there are actually no publications dealing with a systematic development of macro- or microstructures for forming die surfaces for lubricant-free rotary swaging.

1.2.3 Hard coatings for forming dies

The tribological requirements for hard coatings on macro- and micro-structured dies for dry cold forming are highly complex. Microstructured die surfaces in combination with highly dynamically alternating stresses significantly promote coating fatigue. Excellent coating adhesion to the substrate as well as a high toughness, fatigue resistance and hardness are required to avoid wear. Frequently high hardness and high fatigue resistance represent contradicting coating properties.

Generally nitride and carbide coating systems such as titanium nitride (TiN), titanium carbide (TiC), titanium aluminum nitride (TiAlN), aluminum titan carbonitride (AlTiCN) and chromium nitride (CrN) are used for cold-massive forming tools [35]. These coatings offer good protection against abrasive wear but they show increased coefficients of friction against steel or aluminum alloys [36] and are characterized by a strong tendency of adhesive wear [37]. In a dry process design diamond like carbon coatings (DLC) provide both high hardness as well as low coefficients of friction [38]. Hydrogen containing amorphous carbon coatings (a-C:H) show very low coefficients of friction with increasing hydrogen contents [39]. In spite of promising results, a-C:H coatings are mainly applied on forming dies for aluminum alloys due to the comparatively low pressures per unit area [40]. Horiuchi et al. reduced the process forces for dry deep drawing of EN AW-5052 sheets at room temperature and at 200 °C using a-C:H coated dies. Also the formability was improved against uncoated dies in the lubricated state [41]. Abraham et. al achieved a significant reduction of the adhesion of aluminum due to deposition of a-C:H(:Si) coatings on the cold working steel 1.2379 compared to uncoated substrates [42]. The low tendency of aluminum adhesions and other metals to a-C:H coated surfaces is explained by the saturation of carbon bonds by hydrogen or hydroxyl groups [43]. Examination of dry and semidry drawing with DLC-coated dies was studied [44]. The application of a-C:H coated tools for cold massive forming of steel is limited due to a catalytic decomposition of the carbon coatings in contact with iron and also due to higher mechanical loads which significantly depends on the kind of steel to be formed.

2 Methods and Materials

2.1 FEM-Modeling

The 2D-axisymmetric model consists of a die and a workpiece and is implemented with the software ABAQUS 6.13-1, see Fig. 3a. The die is modeled as rigid body and consists of two sections, the reduction zone (I) as well as the calibration (II) including exit zone (III). Thus, different friction coefficients between the workpiece and the die section can be defined. Different coefficients of friction from 0.1 to 0.5 are investigated. Good results in cold metal forming simulations are achieved by a simple friction model with penalty formulation and the Coulomb coefficient of friction [45]. For the fast and dynamic process, the numerical method is based on ABAQUS/Explicit. After the feeding of the first 35 mm of the workpiece (tube and rod) in the swaging unit, the die is completely filled and the process is analyzed. In consequence, only the first 35 mm are provided with a fine mesh. The chosen elements are 4-node bilinear axisymmetric quadrilaterals with reduced integration and activated hourglass control. The mesh size is as large as possible and as small as needed (0.5 x 0.5 mm^2) in order to limit the computation time. Preliminary investigations showed that these constraints do not falsify the results. The workpiece is modeled with an elastic-plastic isotropic material law with parameters from literature [46]. The investigated geometries for the structured reduction zone are sine shapes. The varied parameters of the sine are the wavelength $\lambda = 0.9, 1.1, 1.3$ mm and amplitude $A = 30, 40, 50, 100, 150$ µm. Furthermore, sinewave structures were not only considered with constant amplitude over the wavelength, but also graded structures. In this case the amplitude of the structure decreases towards the calibration zone. This graded structure was only examined for a wavelength of $\lambda = 1.3$ mm and an amplitude of $A = 50$ µm. The strength of the gradation can be described by a structure value S, which can be calculated from the sum of all amplitudes which are in contact with the workpiece. This value also depends on the initial and final workpiece diameter. In the example for the forming procedure from $d_0 = 20$ mm to $d_1 = 15$ mm, $\lambda = 1.3$ mm and $\alpha = 10$ ° eight waves are engaged, see Fig. 4. The coefficient of friction in the reduction and calibration zone is fixed to $\mu = 0.1$ for all simulations derived from the intended coating of the die.

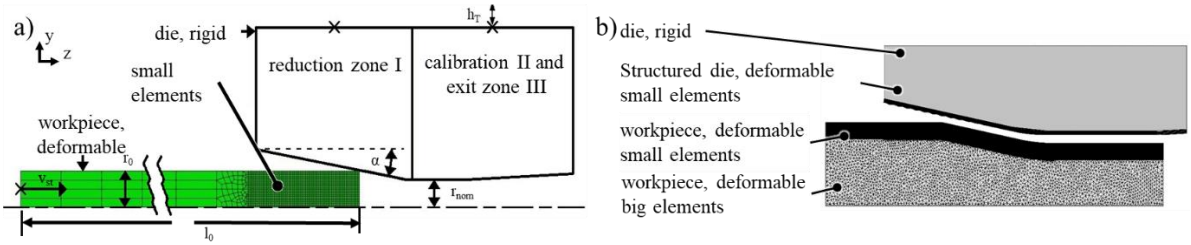

Fig. 3: FEM-model: a) 2D-axisymmetric model and b) planar model, cf. [47]

For the investigation of the elastic-plastic behavior of the die, the 2D-axial-symmetric model is only conditionally suitable. Therefore, a planar model was used, where the upper layer of the die and the whole workpiece was implemented as a deformable body, see Fig. 3b. For the deformable part of the die and the upper layer of the workpiece very fine elements (element size at the surface 10 µm) of the element type CPS4R were used [48]. This guarantees the required display of the structure in the die. The workpiece material is steel 1.0038 with the same material parameters as in the 2D-axial-symmetric model. The die material is hardened 1.2379 (60 HRC) [47]. A single stroke with a feed per stroke of $v_{st} = 1$ mm was simulated.

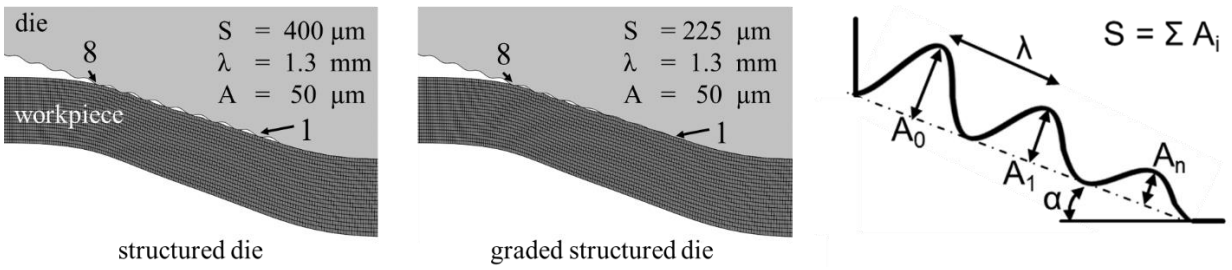

Fig. 4: Different die structures in the reduction zone and structure value S with eight amplitudes in die contact with the workpiece, cf. [47]

2.2 Milling and dimensions of the macro-structure in the reduction zone

Within the scope of the planned structuring of the reduction zone, a complete process chain was developed for manufacturing dies for dry rotary swaging made of the steel X153CrMoV12 (1.2379). The die blanks were mechanically cut from the cold working steel. The geometry is generated by 3-axis milling with a 12 mm

diameter ball end milling tool in the soft state. The pre-machined dies were then heat treated to an overall hardness of 60 ± 2 HRC and the related die distortion was compensated by a subsequent grinding of the external geometry. The machining of the final die geometry was also carried out by means of 3-axis hard-milling with ball end milling tools. The 3-axis hard-milling of the macro-structure in the reduction zones finally was achieved by a change to smaller diameter ball end milling tools (diameter between 0.2 mm and 1.0 mm) [49].

For the examination of different dies, unstructured die sets with smooth reduction zones as well as macro-structured dies in the reduction zone were milled. The basic geometry was obtained by measuring the geometric dimensions of the conventional dies. These data were implemented as a CAD model. The structured die sets with a sine shaped macro-structure in the reduction zone were produced by the 3-axis hard-milling mentioned above. The structure exhibited a wavelength of $\lambda = 1.3$ mm and an amplitude of $A = 0.15$ mm and 0.05 mm as well as a graded structure with changing amplitude towards the calibration zone. The structural parameters were derived from results of 2D finite elements simulations.

2.3 Deposition and properties of amorphous carbon coating systems

A multi-layered PVD-Cr/CrN_x(Cr,W)C_y/a-C:H:W/a-C:H coating system was chosen as coating system for rotary swaging dies due to its high wear resistance, its good adhesion to the steel substrate X153CrMoV12 and the low coefficient of friction against the aluminum and steel workpiece materials. The maximum die surface temperatures for dry forming in stationary state is expected not to exceed the degradation temperature of about 400 °C for this coating system. The mechanical properties of the a-C:H coating system were increased to withstand critical local mechanical overloads. The coating system was applied by reactive magnetron sputtering using the industrial PVD coating device CemeCon CC800/9 SinOx. Fig. 5a shows the target configuration used for deposition of the coating system. Detailed information on specific process control, influence of parameters and the resulting coating properties can be found in [50]. The coating design and primary functions of each layer are illustrated in Fig. 5 b and c.

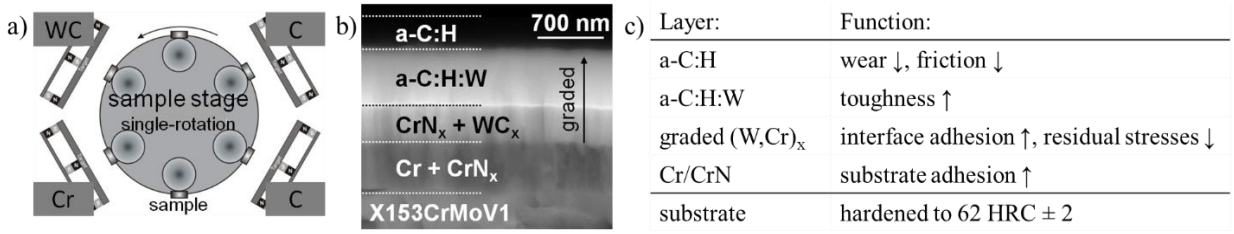

Layer:	Function:
a-C:H	wear ↓, friction ↓
a-C:H:W	toughness ↑
graded $(W,Cr)_x$	interface adhesion ↑, residual stresses ↓
Cr/CrN	substrate adhesion ↑
substrate	hardened to 62 HRC ± 2

Fig. 5: Multi-layered tungsten doped multi-layered a-C:H coating system: a) used target configuration, b) applied single layer design and c) primary single layer functions of the Cr/CrN_x/(Cr,W)C_x/a-C:H:W/a-C:H coating system, according to [50]

Several PVD-Cr/CrN_x/(W,Cr)C_x/a-C:H:W/a-C:H coating systems with a total thickness of about 2.0 µm were deposited onto various dies for dry rotary swaging tests. The Cr/CrN_x layers are used as bonding agent for the amorphous coating layers to the hardened cold working steel substrate X153CrMoV12 (1.2379). Doping of the amorphous carbon layer with tungsten (a-C:H:W) results in a reduction of the residual coating stresses which increases the toughness, respectively the fatigue resistance of these layers [51, 52]. In addition, a smooth transition from metallic CrN_x/(W,Cr)C_y layers to the covalent bound amorphous carbon layers (a-C:H:W) improves the adhesion strength between these layers [53, 54]. This layer is also a graded one in which the WC target power is linearly reduced until the a-C:H top layer is free of tungsten. The tungsten-free a-C:H top layer decreases the adhesive wear (cold welding) as well as the coefficient of friction [50]. This coating system will be denoted as "a-C:H:W/a-C:H" hereinafter.

2.4 Experimental procedures – rotary swaging

Rotary swaging experiments were carried out to characterize different die sets with different functionalization states under lubricated (Condocut KNR 22) and non-lubricated (dry) process conditions. Both experiments were carried out with steel (1.0038) and aluminum (3.3206) tubes, whereby the initial diameter $d_0 = 20$ mm with initial wall thickness $s_0 = 2$ mm was always kept constant. The tubes showed standard deviations of approx. ±20 µm in diameter. Four different feed rates were applied, $v_f = 500$ mm/min, 1,000 mm/min, 1,500 mm/min and 2,000 mm/min. All other process parameters, such as the setting of the swaging head lubrication, the workpiece clamping, the stroke frequency $f_{st} = 35.57$ Hz and the stroke height $h_T = 1$ mm, were kept constant [55].

Five tubes were formed per parameter variation. In the lubricated experiments, all five workpieces could be formed in a row. For rotary swaging tests without lubricant, the swaging unit had to be stopped each time

between the individual repeat trials in order to inspect the dies and also to exclude the influence of particles from the previous experiment. Before each dry test the swaging unit was wiped out and each individual die and the workpiece was cleaned with ethanol to remove oil residues. Residual oil film thicknesses below 100 nm, which can be achieved with such a cleaning, were defined as conditions for dry forming [56].

After the experiments, the recorded process data were evaluated. By means of strain gauges at the outer ring of the swaging head, a qualitative value for the radial process force was averaged over the stable process phase, i.e. when the dies are in full engagement with the workpiece. Furthermore, the displacement of the feed system represents one of the most important process values. The axial reaction force F_A cannot be measured directly but the linear direct drive is subject to a small push-back motion Δx at each die stroke. In this way, F_A can be qualitatively determined. For this purpose, the maximum back motion Δx was determined at each stroke, the point in time of which was determined by means of the strain gauges. This value was also averaged over the stable process phase.

The quality of the workpieces was also assessed. The roundness deviation was determined by three measurements between 40 and 50 mm from the tip and another three between 70 and 80 mm from the tip. These were then averaged for each sample. The surface quality was evaluated using microscope images (VK-X200). Four regions per sample were examined, two measurements each at 40 mm and 80 mm from the tip, the second of which was taken after rotating the sample by 180 °. In the measurements, the roughness Sa was then determined for six fields with a size of 100x100 μm^2 using the software VK-Analyzer according to ISO 25178. These were then averaged for all four images per sample.

3 Results

3.1 Application testing of conventional dies in dry forming

All tests were carried out with and without lubricant using S235 (WKN 1.0037) and AlMgSi0.5 (WKN 3.3206) tubes with a wall thickness s_0 = 2 mm applying the same deformation degree (d_0/d_1 = 20/15 mm). A commercial die set made of the powder-metallurgical ASP2023 steel was used. The commercial dies were coated with a thermally sprayed WC-Co coating with a rough surface topography with a surface roughness Sa of approx. 2.0 µm in the reduction zone and a surface roughness Sa of approx. 0.5 µm in the calibration zone, see Fig. 6a.

For the S235 steel workpieces investigated, the process induced back pushing depends primarily on the lubrication condition and the reduction zone of the die, see Fig. 6d. The dependence of the axial process force on the feed rate decreases in the dry process. Especially for the higher feed rate the back pushing is lower than in the lubricated process. This observation can be explained by the increased friction of dry machining.

Another function that is omitted in dry machining is the flushing of abrasive particles in the deformation zone. It can be assumed that the changed friction properties will result in an additional generation of particles [57]. These particles settle in the WC-Co layer [58]. Furthermore, large quantities of abrasive particles can be observed in the calibration zone of the dies, compare Fig. 6a and b. Thus, the function of the layer to adjust the friction as well as the function of the die in the process is affected [55].

When forming aluminum without lubricant, the first specimen immediately showed an extreme tendency for aluminum adhesion to the die steel. The WC-Co layer was clogged with aluminum over a large area and thus completely lost its function. The calibration zone also showed strong aluminum adhesion, see Fig. 6c [50]. This led to an irreversible damage of the die set. The WC-Co layer had to be completely removed and renewed.

Furthermore, in-process temperature measurements were carried out under lubricated (wet) and dry forming with different feed rates. The temperature increased from the minimum to the maximum feed rate of about 10 °C. These small increases could only be determined by comparing lubricated and non-lubricated forming. Immediately after machining, no difference in temperature between forming with and without lubricant could be detected on the outer surface of the steel tubes. Furthermore, the temperature measured on the surface was lower than that inside the tubes [59].

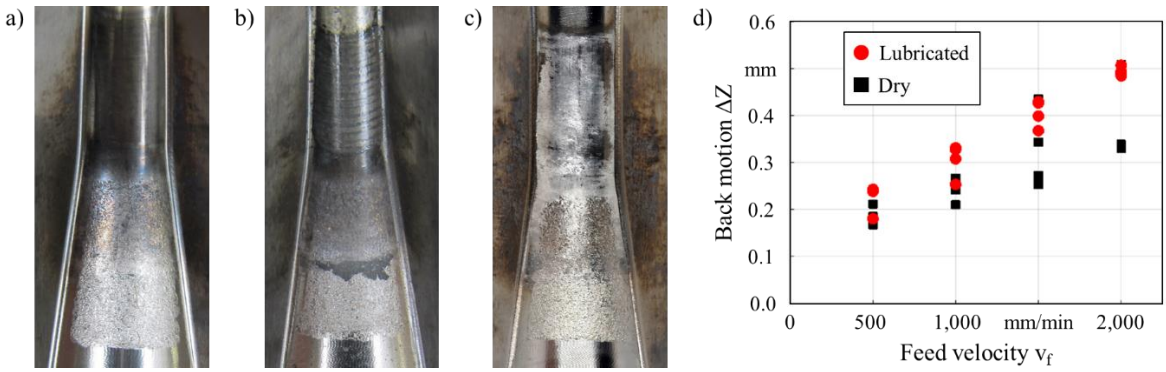

Fig. 6: Dry rotray swaging with conventional dies: a) clean die, b) die after dry forming of steel with v_f = 1,000 mm/min, c) die after dry forming of aluminum with v_f = 1,000 mm/min and d) back motion for forming of steel, cf. [47].

3.2 FEM-Simulations of smooth and structured dies

With the FE-program ABAQUS a 2D-axial-symmetric process model was built to determine the influence of friction and geometric elements (macro-structure in the reduction zone of the die) on the forming behavior. The forming dies were divided in the model into two areas, the reduction zone, where the essential forming takes place, and the calibration zone for the final shape and surface generation. In these two zones, different coefficients of friction should be adjustable in order to design the functionalized dies in the best possible way. As a result, the process forces and the material flow were evaluated. First of all, the process forces as a function of friction were investigated, since dry rotary swaging in particular changes the tribological conditions. This influence on the radial and axial process forces is shown in Fig. 7. The maximum process forces (F_A and F_R) from the simulation are shown, which are normalized with the process forces in case of a lubricated process (tribological conditions constant over the die: μ = 0.1/0.1; coefficient of friction in the reduction zone and calibration zone).

It the coefficient of friction in the reduction zone increases, the axial process forces decrease and the radial process forces increase. With different coefficients of friction in the reduction and calibration zones, the main influence results on the axial process force comes from the reduction zone, whereby the radial process forces are less influenced than the axial process forces. By increasing the friction in the reduction zone and reducing the friction in the calibration zone, the lowest process forces, combined axially and radially, are achieved. Furthermore, it was found that by increasing the feed rate and thus the feed per stroke, the trend is maintained, but the total process forces increase.

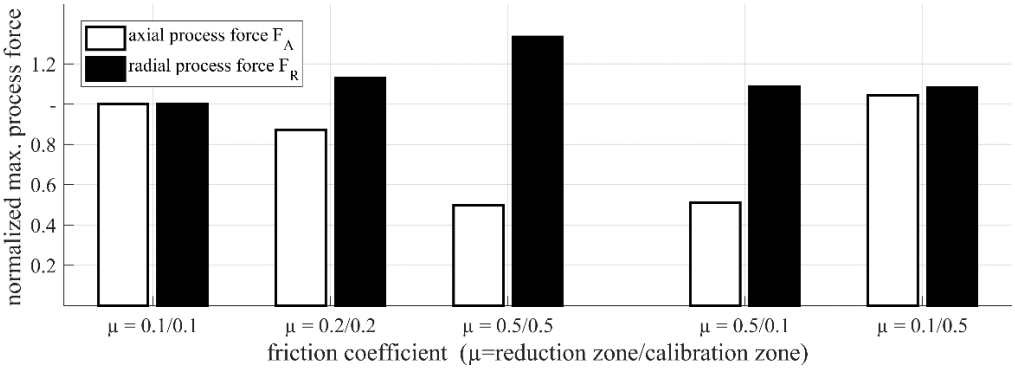

Fig. 7: Normalized maximum process forces for rotary swaging of steel with different tribological conditions, cf. [47]

The material flow is separated at the neutral plain into the axial material flow in the feed direction (towards the calibration zone) and against the feed direction. The further the neutral plain is moved to the beginning of the reduction range, the larger the effect on the maximum achievable degrees of deformation and feed rates. Fig. 8 shows three exemplary results, with the axial contact length in the reduction range set at 100 % and the position of the neutral plain is given as ratio [60]. With friction coefficients of μ = 0.1, the neutral plain is relatively close to the calibration zone. At high friction coefficients, however, the neutral plain is shifted further into the reduction zone. The most favorable effect is achieved with high friction coefficients in the reduction zone and low friction coefficients in the calibration zone. This also corresponds to previous practical experience with rotary swaging with lubricant and dies with WC-Co in the reduction zone as well as polished calibration zone.

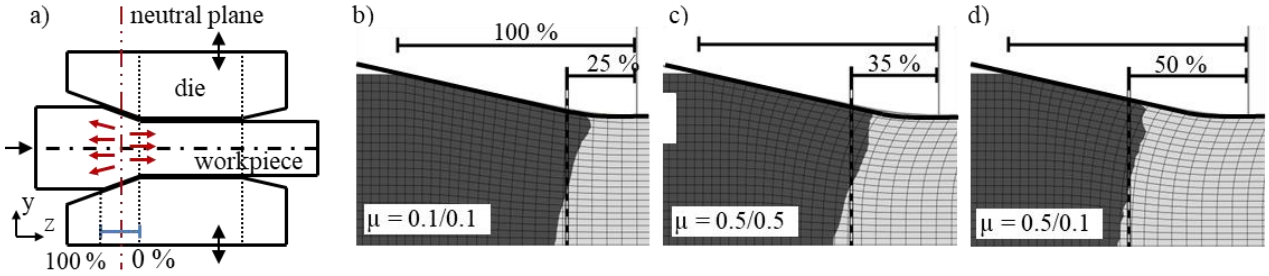

Fig. 8: Neutral pain for forming with different tribological conditions (friction μ = reduction zone/calibration zone): a) schematic representation, b) exemplary neutral plane for friction μ = 0.1/0.1, c) μ = 0.5/0.5 and d) μ = 0.5/0.1, cf. [60]

In the next step, the influence of structuring elements (sine) in the reduction zone on the forming behavior was investigated at a friction coefficient of μ = 0.1 and a constant die angle α = 10 °. For this purpose, different wavelengths, λ = 0.9/1.1/1.3 mm and different amplitudes A = 0.03/0.04/0.05/0.1/0.15 mm were set. The simulation calculations show that both the amplitude and the wavelength have an influence on the forces. An increase in amplitude and wavelength causes a decrease in the axial reaction force, see Fig. 9. The radial force also decreases with increasing wavelength, but an influence of the amplitude is not noticeable.

However, it is to be expected that the type of the structure will have an influence on the quality of the workpiece, especially the surface [61]. Therefore, alternative structures were investigated which have a gradation. This is also of interest with regard to the coating. It can be assumed that the shape of the structure will have an influence on the adhesion and delamination tendency of the coating when the structure and coating are combined on the die [62]. For the investigation of the gradation, i.e. a structure that can be changed over the reduction zone of the die, the sine structure is considered. The structure with the largest wavelength λ = 1.3 mm and an amplitude of A = 50 μm is used [63].

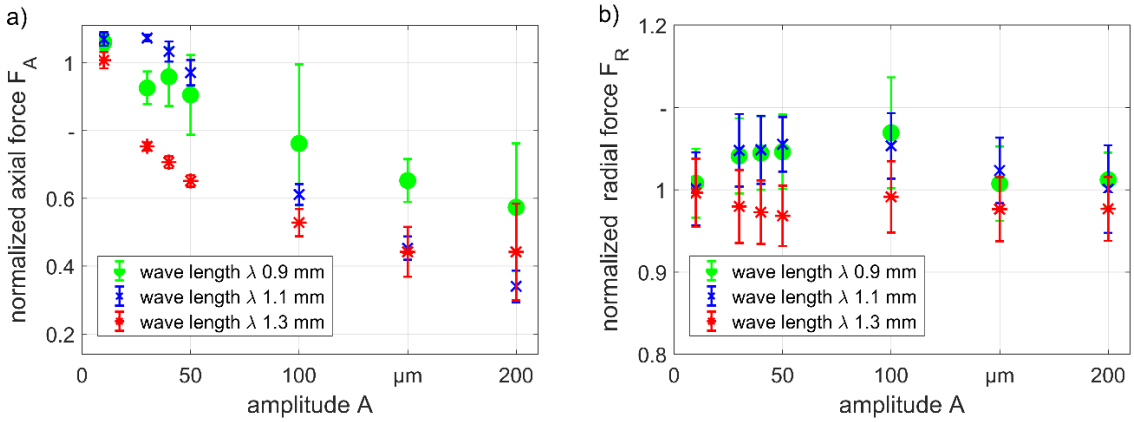

Fig. 9: Simulated process forces with structured and to unstructured dies (100%): a) axial reaction force F_A and b) radial force F_R, cf. [63]

The normalized axial process force F_A as a function of the structure value S for three different tribological conditions is shown in Fig. 10. The averaged maximum axial process forces per stroke during the stable phase of the process are shown. The result of the simulation with the friction coefficient μ = 0.1 and a structure value of S = 0 μm serves as the basis for the normalization of the process forces. A structure value of S = 0 μm means that no structure contacts the workpiece (smooth reduction zone of the die), whereas an increasing structure value indicates more engaging structure in length and/or height.

With increasing structure value S the axial process force decreases. This can be seen at the lowest friction coefficient over the entire variation of the structure value. At a slightly higher friction value of μ = 0.15, the maximum reduction of the axial process force is already reached at S = 180 μm. Even at the highest coefficient of friction, the axial process force no longer decreases from this structural value. The effect of the structure for higher coefficients of friction is significantly lower when normalized to the lowest coefficient of friction.

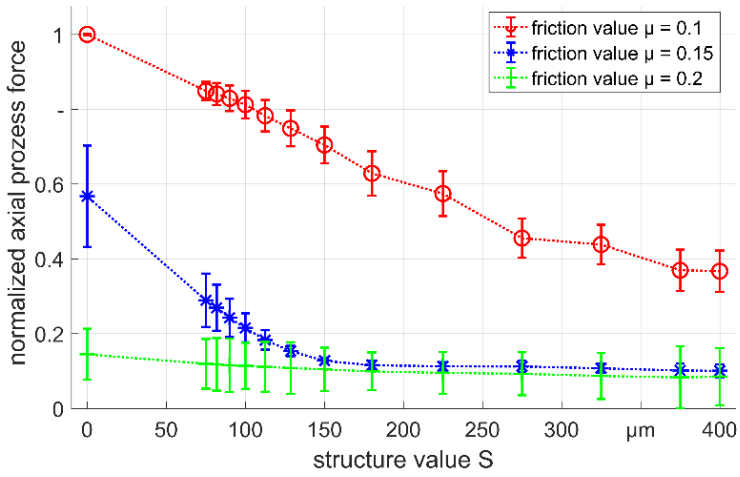

Fig. 10: Normalized process forces for the forming of steel tubes with different graded die structures (structure value S) in the reduction zone, cf. [64]

Another subject that can be investigated by FEM is the occurring of strain rates in the workpiece. This can provide information about where and which loads occur in the workpiece and in the contact zone between workpiece and die. This knowledge can reveal information about the coating behavior, such as adhesion.

Fig. 11a shows the strain rates in the workpiece for rotary swaging of steel bars with dies without structure in the reduction zone and with a low coefficient of friction of $\mu = 0.05$ ($v_f = 2{,}000$ mm/min). The selected point in time is about 82 % of the stroke in the stable process phase. This is where the maximum strain rates occur. High strain rates were identified at three points. One of the points (C) is located in the symmetry axis of the workpiece, the other two (A and B) are located on the surface in contact with the die. The positions of points A and B on the surface are the first point of contact in the reduction zone (A) and the transition from the reduction zone to the calibration zone (B). These two positions are therefore the tribologically most demanding. This means that the dies are subjected to very high loads, as the material formed most rapidly here. It was also shown that the elements here are elongated most, which means that most of the new surface is created here. [65].

The strain rates were investigated using the planar simulation model for dies with macro-structured reduction zones ($\mu = 0.1$; $v_f = 2{,}000$ mm/min). It was found, that in a wave of the structure where the workpiece material comes into contact with the die for the first time, areas with increased strain rates are present. These areas migrate into the valley of the structure during a stroke. This migration fits also where the first point of contact moves, see Fig. 11b. Fig. 11c shows an example of the von Mises equivalent stresses in the sine-structure. Here it can be seen that at the first contact point, the areas of highest alternating stress occur on the peaks of the structure, which can lead to damage such as layer delamination [62]. The results of the FEM simulations show in which critical areas the highest die stresses and a strong tendency to cold welding can be found.

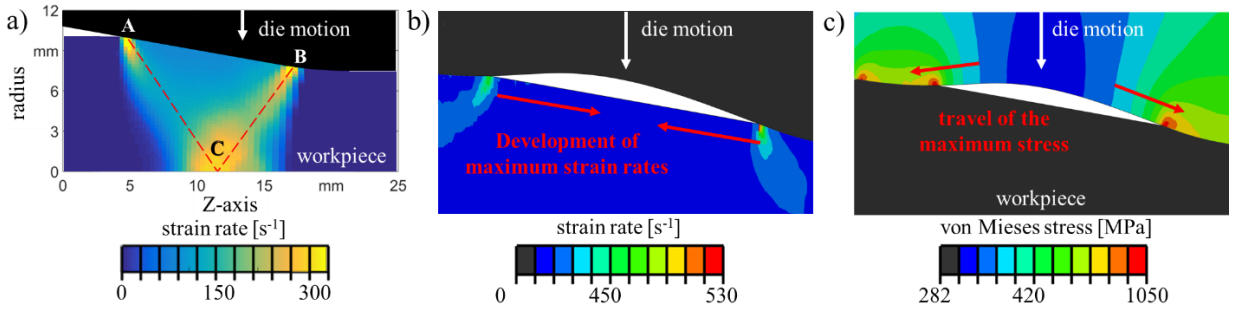

Fig. 11: Strain rates in the workpiece material and stress in the die during the process: a) while forming with smooth dies, cf [65], b) while forming with smooth dies and c) von Mises equivalent stress of the macro-structure of the die, cf. [47]

In planar FEM, the plastic deformation of the structure can also be evaluated. In this way it can be checked whether local plastic deformations of the structure are possible due to the exceeding of critical stresses. This would promote layer delamination and thus wear. Fig. 12 shows that the predominant deformation in the workpiece occurs at the point of contact with the structure. Since the die is a graded one, the comparative plastic strain in the left-hand structure peak (the larger of the two structure peaks shown) is significantly higher than in the second structure peak. In the die, however, only minimal deformation of the boundary elements is ob-

served. The maximum deformation is PEEQ = 0.13 %. The simulation results showed a permanent displacement of the nodes of the elements of only 50 nm. With reference to a failure of the die (or of the multilayer system), this displacement is not critical [62].

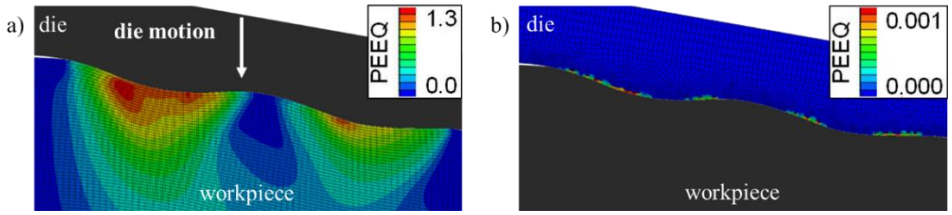

Fig. 12: Equivalent plastic strain during one single stroke: a) in the workpiece material and b) at the die surface at the highest feed rate, cf. [47]

3.3 Tribological model test rig for dry rotary swaging

Cylinder compression tests were carried out on a Schenck Trebel RM 250 tensile compression testing machine to determine the friction factor m of structured samples. Cylindrical samples with a diameter of 36 mm made of tool steel 1.2379 hardened to 62 HRC were used as die samples. One unstructured pair of die samples as a reference and nine macro-structured pairs of die samples with concentric sinusoidal surface structures were manufactured by hard turning. Three wavelengths λ = 0.9 mm, 1.1 mm and 1.3 mm each with three amplitudes A = 0.03 mm, 0.04 mm and 0.05 mm were combined in a full factorial design of experience plan (DoE). The characterization of shape and surface roughness of the manufactured die samples was carried out by confocal microscopy. The arithmetical mean height of all samples was Sa = 72 nm (empirical standard deviation s = 27 nm). Cylinders (initial diameter d_c = 10 mm, initial height h_c = 10 mm) of structural steel S235 and aluminum AlMgSi1.0 were used as workpiece samples. These were compressed to a height of 6 mm at a speed rate of 1 mm/min. Lubricated and dry cylinder compression tests were performed with the unstructured reference die sample pair and with a structured die sample pair (λ = 0.9 mm, A = 0.05 mm). The oil Wisura ZO 3368 was used for lubrication. The height as well as the maximum new diameter of the deformed workpiece samples were measured with a caliper and the friction factor was determined according to the method of Ebrahimi and Nahafizadeh [66]. The results shown in Fig. 13 display the mean values as well as the minimum and maximum values from three repeat tests.

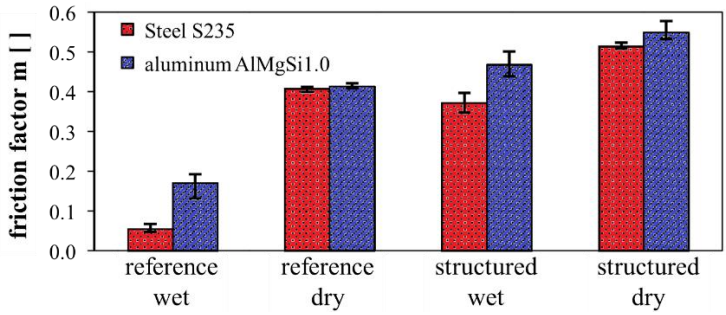

Fig. 13: Comparison of the measured friction factors m of an unstructured reference and a structured die sample (sinusoidal macro surface structure, wavelength λ = 0.9 mm, amplitude A = 0.05 mm) each dry and lubricated during cylinder compression tests of steel and aluminum samples

The tests carried out dry generally show higher friction, see Fig. 13. A macro-structured die sample surface leads to an increase in friction; this applies in particular to the lubricated tests [60]. Fig. 14 shows the influence of structure amplitude and wave position on the friction factor m for dry cylinder compression tests. Higher amplitudes of the sinusoidal structure lead to an increase of the friction factor. This is attributed to a stronger forming of the workpiece sample material into the macro-structure of the die sample and thus an obstruction of the relative motion of material. A further increase in amplitude should tend to further increase the friction factor. The influence of a wavelength variation in the size range around λ = 1.0 mm on the friction factor is of minor importance. When transferring the gained insights to rotary swaging dies, sinusoidal structures with longer wavelengths, e.g. λ = 1.3 mm, can be used without a significant drop in the friction factor. This allows for the use of ball end milling tools with larger diameters which reduces the risk of tool breakage and simultaneously increases the material removal rate.

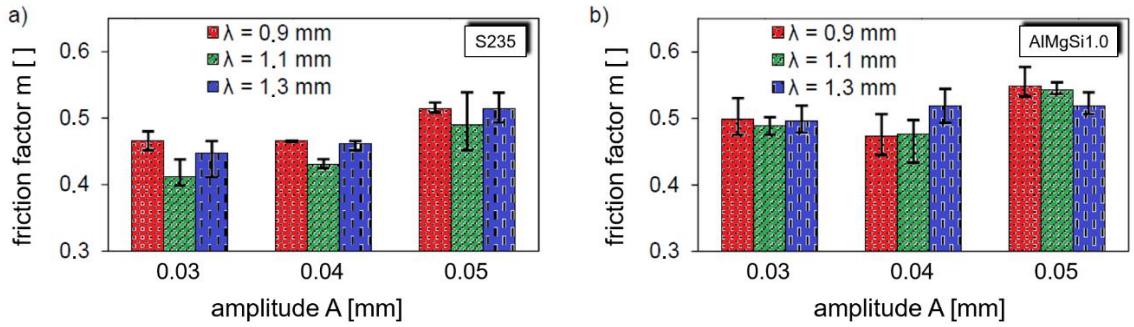

Fig. 14: Measured friction factors of die samples with concentric, sine shaped surface structure as a function of amplitude A at dry cylinder compression: a) S235 and b) AlMgSi1.0

For a process specific determination of the friction properties of structured and hard coated die samples, a tribological model test rig was developed [67], which reproduces the contact geometry between the rotary swaging die and the workpiece as well as the impulse like loads of the rotary swaging process with simultaneous access to the measurement technology. Direct measurement of the influence of structured and hard coated die surfaces on the process forces during real rotary swaging is only possible with a high degree of technical effort due to the limited metrological accessibility, e.g. for piezoelectric force sensors. In addition, a new entire die set must be manufactured for each surface modification to be investigated. The developed and assembled tribological model test rig comprises a die sample and a workpiece sample in tribological contact at a wedge angle of $\alpha = 10$ °, see Fig. 15.

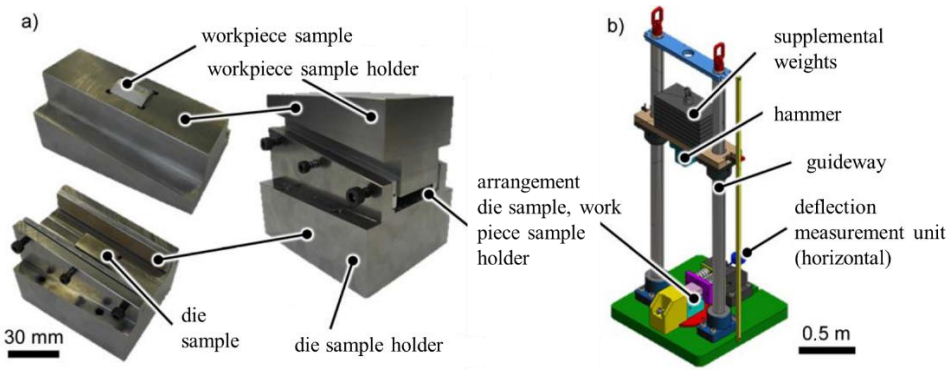

Fig. 15: Tribological model test rig: a) workpiece and die sample holder in wedge arrangement and b) general view, cf. [67]

The effective contact area between die and workpiece sample is 100 mm^2. The impact of a guided, variable dead weight on the sample holder can be applied repeatedly in a range between 10 kN and 1,000 kN. The measurement of the maximum excitation force $F_{R,max}$, which is corresponding to the radial force F_R in the rotary swaging process, is carried out using a piezoelectric force sensor. The maximum reaction force $F_{A,max}$, which is corresponding to the axial rejection force F_A in the rotary swaging process is measured indirectly via a deflection measurement of the workpiece sample holder against a spring assembly using a dial gauge with drag pointer, see Fig. 16. Based on the real process, this feature allows for a relative movement between the die and the workpiece sample. The design of the test rig is based on the process forces determined in simulation calculations and the estimation of the maximum excitation force [60]. The test rig was used to examine various die samples for their process-specific friction properties. The nominal excitation force for this test was 230 kN. The measured excitation force $F_{R,max}$ was lower due to the forming work performed on the workpiece sample.

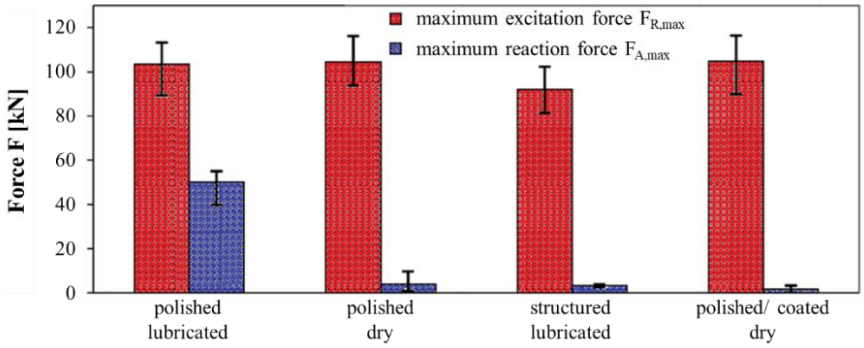

Fig. 16: Detail of the tribological model test rig for the process-specific determination of the friction properties of structured and coated die samples

As expected, the lubricated reference test shows a high reaction force. In contrast, the results for the dry tests are at a similar excitation force level. The macrostructure causes a reduction of the reaction force compared to the polished surface. The highest friction was found for the coated sample. Thus, the function of the test rig was successfully demonstrated. In addition to the investigations of the reduction zone, different microstructures can also be tested for the calibration zone to increase the functionalization of the dies, see section 3.6.2.

3.4 Development of tungsten doped a-C:H coating systems

For all coating systems, six Rockwell-C adhesion tests according to VDI guideline 3198 and 10 scratch tracks according to DIN EN 1071-3 were carried out in order to determine the coating adhesion strength to the substrate. The determination of the total coating thickness and the single layer thicknesses was carried out by six calotte grindings on each specimen.

Fig. 17 shows the measured critical load Lc2 and the adhesion class HF as a function of several PVD process parameters. The average critical load Lc2 was about 40 N and the adhesion class HF for all coating variants was between HF 1 and HF 3. A reduction of the tungsten carbide target power $P_{WC\ target}$ leads to an increased substrate adhesion. Especially at 0.8 kW a significant increase of Lc2 to about 57 N was observed. With increasing $P_{WC\ target}$ a linear increase of the coating thickness from 1.9 to 2.8 µm was observed, which could also have an influence on the determination of the coating adhesion. For a more precise analysis of all process parameters further investigations are necessary. The reduction of the bias voltage U_{bias} from -150 to -75 V leads to an increase of the coating adhesion. The variation of the ethine flow rate $\Phi(C_2H_2)$ showed no clear correlation to the coating adhesion. Furthermore, an influence on the ethine flow rate on the resulting coating thickness could not been observed.

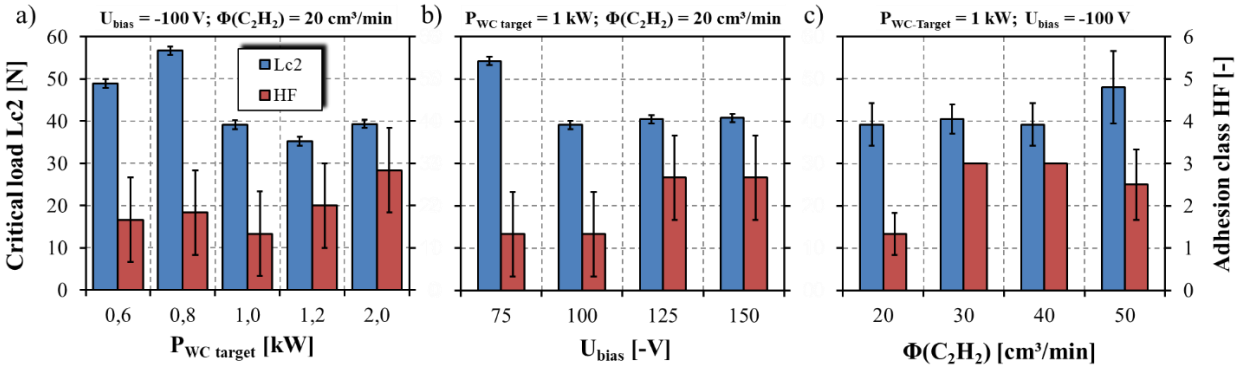

Fig. 17: Critical load Lc2 and adhesion class HF as a function of the PVD process parameters: a) $P_{WC\ target}$, b) U_{bias} and c) $\Phi(C_2H_2)$

The indentation hardness H_{IT} and the elastic modulus E_{IT} was measured according to DIN EN 14577-1. On each specimen 49 single indentations with a maximum indentation force of 10 mN were carried out. The 10 % indentation depth rule (Bückle rule) was fulfilled for most specimens. Fig. 18 shows the resulting indentation hardness H_{IT} and indentation modulus E_{IT} as a function of selected PVD process parameters. For increasing target power $P_{WC\ target}$ from 0.6 to 1.2 kW a slight reduction of H_{IT} is observed. At 2.0 kW an increase to approx. 20 GPa occurred. E_{IT} remains more or less constant at approx. 200 GPa for $P_{WC\ target}$ = 0.6 to 1.2 kW. Both, H_{IT} and E_{IT} increase with increasing U_{bias} from 16 to 20 GPa respectively 186 to 210 GPa. An increase of the ethine flow rate $\Phi(C_2H_2)$ leads to a decrease of H_{IT} and E_{IT}. For all PVD process parameter variations H_{IT} remained above 14 GPa and E_{IT} remained above 150 GPa.

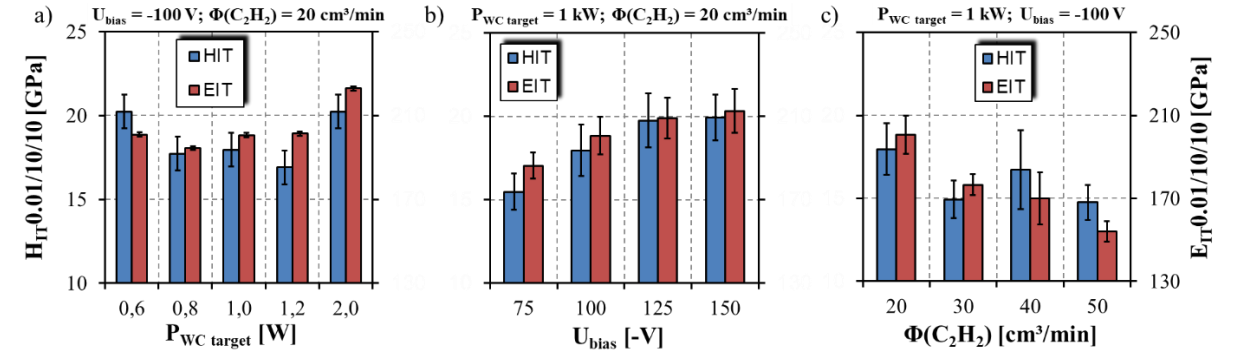

Fig. 18: Indentation hardness HIT and elastic modulus EIT as a function e of the PVD process parameters: a) $P_{WC\ target}$, b) U_{bias} and c) $\Phi(C_2H_2)$

Pin-on-disc tribometer tests were carried out under dry testing conditions of uncoated and coated steel discs (hardened 1.2379), in order to determine the coefficient of friction (CoF) and the coefficients of wear for the pin (k_{pin}) and for the uncoated and coated steel discs ($k_{coat.}$). Furthermore, a representative a-C:H:W coating system with an a-C:H top layer and without a-C:H top layer (a-C:H:W) were tested. The representative settings for both coating systems can be found above the diagrams (U_{bias} = -100 V; $\Phi(C_2H_2)$ = 20 cm³/min; $P_{WC\ target}$ = 1 kW). Hemispherical pins with a diameter of 6 mm made of the construction steel S235 and the aluminum alloy AlMgSi0.5 were used. In order to achieve process-related test conditions, the average surface pressure calculated from the FEM simulations was converted into the corresponding normal forces for the pin-on-disc tests. An initial FE simulated Hertzian pressure of 1,200 MPa for the S235 pins and an initial pressure of 340 MPa for AlMgSi0.5 resulted in a normal force of 12 N for the S235 steel pins and 5 N for the AlMgSi0.5 pins. The sliding velocity was determined from the relative nodal displacement speed in the calibration zone in stationary state, calculated from the FEM model. The velocity was kept constant at 0.25 m/s for all tests. Fig. 19 represents the resulting CoF curves depending for a long-time test of 20,000 cycles resulting in a sliding distance of 1.5 km.

Fig. 19 shows the CoF of an uncoated and a-C:H:W and a-C:H coated steel disc tested against AlMgSi0.5 and S235 pins. The CoF is about 0.7 for the uncoated steel disc against AlMgSi0.5 and about 0.9 against S235 pins. The a-C:H:W layer significantly reduces the CoF to approx. 0.4 against AlMgSi0.5 and to approx. 0.3 against S235 pins. A further decrease of the CoF could be observed for the coating system with a tungsten free a-C:H top layer. The CoF achieves more or less constant levels after 5,000 cycles. The a-C:H:W and a-C:H coating systems significantly reduce the friction for both pin materials. The lowest friction was achieved for coatings with a tungsten free a-C:H top layer.

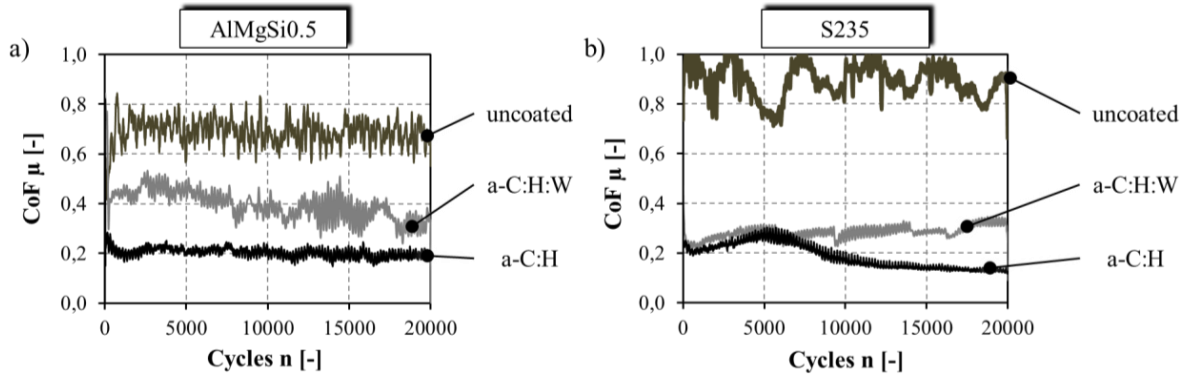

Fig. 19: Coefficient of friction µ (CoF) for an uncoated reference system, a representative a-C:H:W top layer and a a-C:H top layer against: a) AlMgSi0.5 (mat. no.: 3.3206) and b) S235 (mat. no.: 1.0038) pins in pin on disc tests under dry conditions

The coefficients of wear were determined according to DIN EN 1071-13. The wear scars at the tested pins and also the wear tracks on the tested discs were measured by confocal laser scanning microscopy (CLSM). Fig. 20 shows the determined coefficients of wear of the aluminum and steel pins against an uncoated steel disc as reference and the coated steel discs. Both pin materials show a decrease of wear of more than two orders of magnitude due to the amorphous carbon coatings of the discs, see Fig. 20. A significant decrease of the wear coefficient was observed for the coating system with a-C:H top layer, which is also in a good correlation to the lowest coefficient of friction for this coating system.

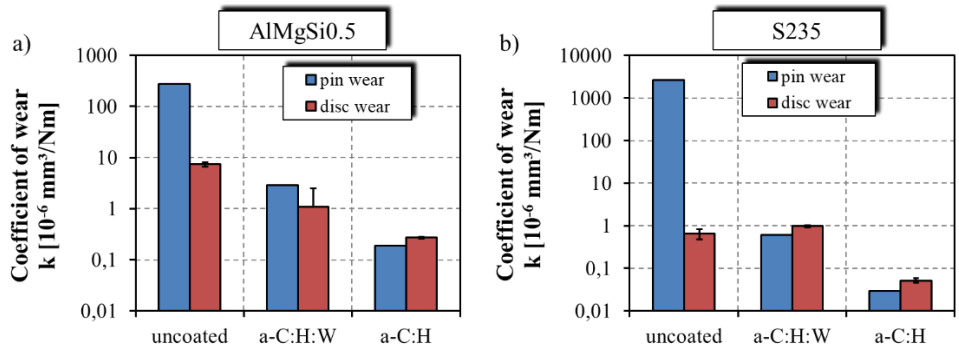

Fig. 20: Coefficients of wear k_{pin} and $k_{coat.}$ against: a) AlMgSi0.5 (mat. no.: 3.3206) and b) S235 (mat. no.: 1.0038) in dry pin on disc tests conditions

Based on these promising results a coating system, denoted as $DLC_{ref.}$, for the application tests in the following sections was used which corresponds to the SEM fracture pattern in Fig. 5b.

In a next step, the target configuration according to Fig. 5a changed by replacing the WC target to a pure W target. In relation to the findings of Fig. 17 and Fig. 18 a stable process window could be defined for a systematical coating development. For this purpose, the layer design remained unchanged. For a systematical development of the investigated coating design a central composite inscribed (CCI) experimental plan with high resolution for describing the main influence factors, 2-fold interactions and to derive regression mathematical models was carried out, see Fig. 21a. The CCI design consists to the design of experiments (DoE). As main influence factors the tungsten target power $P_{W\ target}$, ethine flow rate $\Phi(C_2H_2)$, bias voltage U_{bias} and the graphite target power $P_{C\ target}$ were systematically varied. In total, two identical CCI designs with 26 coating process variations, denoted as DoE-runs, were carried out. The first CCI design was carried out at constant deposition times in order to develop a tool taking the different main factors into account for depositing constant a-C:H:W und a-C:H layer thicknesses for the second main CCI plan. The resulting total coating thickness of all 26 DoE-runs of the main CCI were approx. 2.1 µm ± 0.1 µm. It can be summarized that both the developed tool for the deposition rates is sufficient and all DoE-runs become comparable due to the following experiments. The results presented in the following are excerpts from the main CCI test plan.

By varying the main factors A to D, both the indentation hardness H_{IT} and the indentation modulus E_{IT} change over a wide range, see Fig. 21b. It was possible to set H_{IT} from 8 GPa for the DoE-run 3 to 20 GPa for DoE-run 5. E_{IT} follows the trend of H_{IT}. The modulus increases with increased hardness. Herein, the elastic modulus E_{IT} ranges between 70 GPa for DoE-run 3 to 150 GPa for DoE-run 5.

a)

DoE-run	A: $P_{w\ target}$ [W]	B: $\Phi(C_2H_2)$ [cm³/min]	C: U_{bias} [-V]	D: $P_{C\ target}$ [W]
2	1150	35	50	1500
3	650	85	50	1500
5	650	35	100	1500
7	650	85	100	1500
20	900	97	75	2000
26	900	60	75	2000

b)

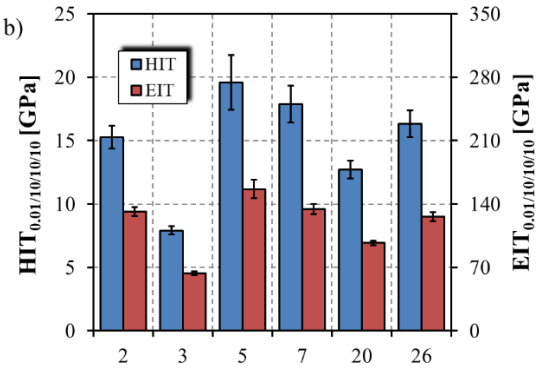

Fig. 21: a) Main factors of the CCI design and b) resulting indentation hardness H_{IT} and modulus E_{IT} of exemplary DoE-runs

The coating adhesion strength was determined by Rockwell-C adhesion tests according to VDI guideline 3198. An image analysis tool was developed to quantitatively determine the relative area of delamination $A_{D,r}$ around the Rockwell imprints by a black and white conversion of the CLSM recorded images, see Fig. 22 a and b. The mandatory requirement of the quantitative image analysis was the automation of a suitable threshold value analysis which is unaffected by the exposure source, the image brightness or image coloring. For the statistical analysis six Rockwell adhesion tests were carried out and subsequently analyzed, see Fig. 22c. The adhesion class varies between HF 1 and HF 3 representing a very good to medium adhesion. In comparison to HF the accuracy of the relative area of delamination $A_{D,r}$ could be improved. The absolute values of $A_{D,r}$ and their standard deviations can be differentiated from each other. In contrast, all standard deviations from HF overlap with the exception of DoE-run 5 which makes an exact assessment of the adhesion less accurate. In Fig. 22d the analyzed $A_{D,r}$ of all DoE-runs are illustrated in correlation to the manual assessed adhesion classes HF of the CCI design. As expected a pronounced correlation on the averaged data of $A_{D,r}$ and HF could be found with a coefficient of determination of 95 %. The regression function is a second-degree polynomial. With this developed method it is possible to assign correct adhesion classes HF along the regression curve of quantitatively measured $A_{D,r}$ for a-C:H(:Me) coatings [68].

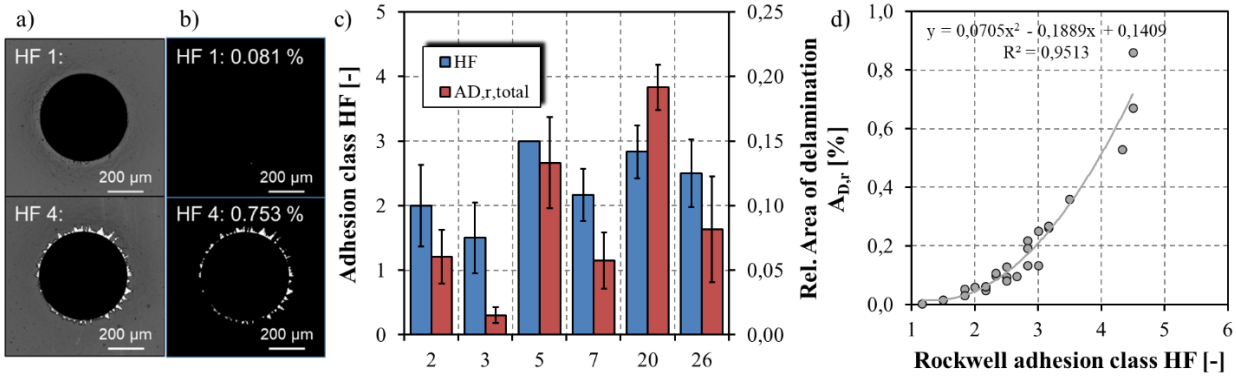

Fig. 22: Functionality of the semi-automatic image analysis tool for Rockwell-C adhesion tests: a) input images, b) back-white conversion with determined optimal threshold value , c) comparison of the manual assessment HF and the quantitative image analysis $A_{D,r}$ and c) correlation curve between HF and $A_{D,r}$ of exemplary DoE-runs [68]

The semi-automatic image analysis tool was extended in terms of analyzing the scratch tracks subsequent to the scratch tests on the CCI design plan carried out [69]. In Fig. 23a the resulting critical loads Lc1 to Lc3 according to DIN EN 1071-3 due to the optical assessment by CLSM are presented for the exemplary DoE-runs. Lc1 is in the range between 9 N for DoE-run 20 and about 18 N for the DoE-run 3. Lc2 varies about 25 N for the DoE-runs 5, 7 and 20 and 40 N for the DoE-runs 2, 3 and 26. Lc3 is located above 90 N for all DoE-runs. As can be seen for Lc2 a unique comparability is not given since only two groups of Lc2 were determined. For this purpose, additional image analysis were carried out at Lc2 for each DoE-run with a partial image length of 900 µm and an image height of 300 µm in order to determine the relative area of delamination $A_{D,r,total}$. The functionality is comparable to the above described method for Rockwell-C adhesion tests, see Fig. 23b. In Fig. 23c $A_{D,r,total}$ is shown for the exemplary DoE-runs. Large differences in $A_{D,r,total}$ can be seen in particular for the DoE-runs 5 and 20 which are characterized by the same Lc2 of about 25 N. The DoE-runs 2 and 7 exhibit the same $A_{D,r,total}$ of 0.51 % whereas Lc2 differs of about 15 N. These results confirm the usefulness of the supplementary description of the coating adhesion by means of image analysis for scratch testing [70].

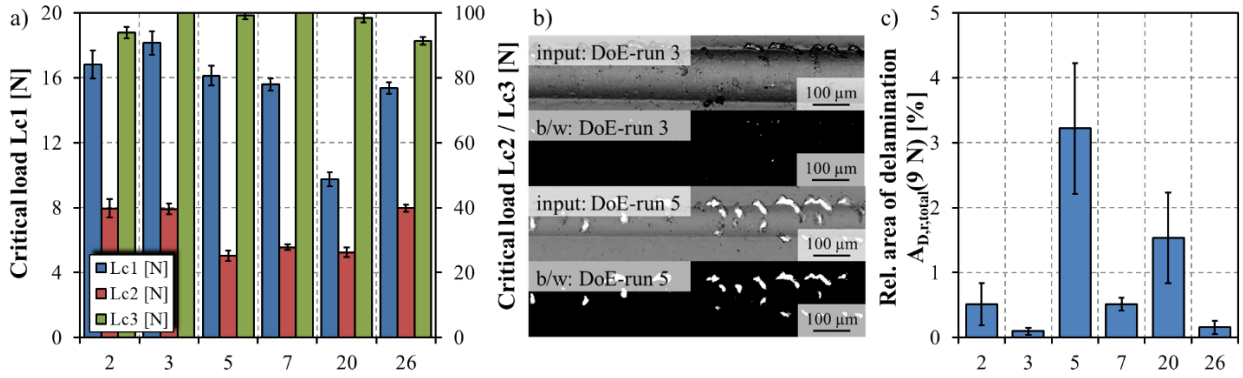

Fig. 23: Scratch test results a) critical load Lc1 to Lc3 analyzed by CLSM, b) functionality of the semi-automated partial image analysis tool for scratch tracks of 900 µm partial length at Lc2 and c) resulting $A_{D,r,total}$ of the quantitative image analysis of exemplary DoE-runs [70]

The residual coating stresses $\sigma_{res.}$ were determined by bending curvatures of single side coated thin steels foils using the equations of the works of Stoney [72], Brenner [73] and Benabdi et al. [74] , see equations (1) and (2). A small film thickness d_f compared to the substrate thickness d_s is assumed as boundary condition for all tested approaches ($d_f << d_s$). Furthermore, purely elastic substrate bending is assumed. In equation (1) the Young's modulus of the substrate E_s, the thicknesses d_f and d_s and the strip bending radius R are considered:

$$\sigma_{res.} = -E_s \cdot \frac{d_s^2}{6 \cdot R d_f} \tag{1}$$

In addition to the Stoney-equation, Brenner et al. have extended the equation by the Poisson ratios of the substrate ν_s and applied coating ν_f and the Young's modulus of the coating E_f:

$$\sigma_{res.} = \frac{\frac{E_S}{(1-\nu_S)} \cdot \left(d_S + \frac{E_f(1-\nu_S)}{E_S(1-\nu_f)} \cdot d_f \right)^3}{6 \cdot R d_s d_f} \tag{2}$$

In Benabdi et al. both variants were considered, with and without Poisson ratios and further film properties. For reasons of comparability ν_s was set to 0.3 [74] and ν_f was set to 0.22 [75]. As E_f the elastic modulus E_{IT} in Fig. 21b was inserted into the equations. For this purpose, 10 tensile strip foils of a thickness of 100 µm made of DC01 steel (mat. no.: 10330) were coated on one side for each DoE-run. Due to the resulting residual coating stresses caused by the layer growth process depending on the different sputter parameters of Fig. 21a, the thin strips are characterized by different pronounced curvatures, see Fig. 24a and b. By the use of this bending method it was possible to calculate the residual coating stresses $\sigma_{res.}$ for the complete CCI design. The resulting strip curvatures were measured by CLSM. Among other, the used formulas take the coating thickness, strip thickness, Young's moduli of both the applied coating system and DC01 material as well as the Poisson ratios into account. The basic requirement for the comparability of $\sigma_{res.}$ is a constant coating thickness for all DoE-runs. This condition is given by the mentioned results of the calotte grindings with minimal deviations below 5 % for the entire CCI design plan.

Fig. 24c shows the determined coating stresses due to the strip bending for several DoE-runs. The stresses vary in a wide range of about +700 MPa to -1,000 MPa. The softest DoE-run 3 shows slight negative strip curvatures and thus tension residual stresses. However, due to the high standard deviations it should be assumed that this coating system is nearly stress-free. A slight correlation could be observed for the presented DoE-runs to the hardness H_{IT} in Fig. 21b. The DoE-runs 5 and 7 exhibit the highest $\sigma_{res.}$ and H_{IT}. At the opposite, DoE-runs 2 and 20 are characterized by low $\sigma_{res.}$ and medium H_{IT}.

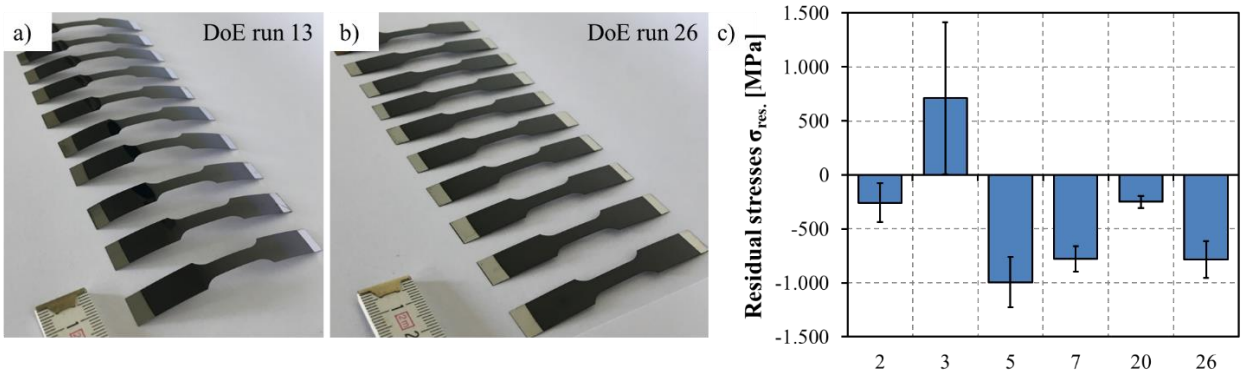

Fig. 24: Exemplary curvatures of one-side coated waisted strip foils: a) DoE-run 13 and b) DoE-run 25 and c) resulting averaged residual stresses by the bending method and the use of the equations of Stoney [71], Brenner [72] and Benabdi et al. [73] of exemplary DoE-runs

For characterization of the fatigue resistance of the coatings, impact tests were carried out using an impact tribometer of the type Apollo NXG of the Impact-BZ / CemeCon GmbH. The impact tribometer operates with the frequencies of 15, 25 and 50 Hz. The impact force can be adjusted between 150 and 1,500 N per impact. The tests were carried out at 50 Hz, all experiments were done twice to check the reproducibility. A Si_3N_4 ball with a diameter of 5 mm was used as impact body for all experiments. To avoid fatigue at the impact balls, a different ball for each DoE-run specimen was used. The balls were rotated between the individual measurements to avoid influences of ball fatigue or residual coating adhesions at the ball contact area. The approach for determining the impact fatigue resistance was the procedure according to the works of Bouzakis et al. [76]. The assumption of this approach is that the plastic substrate deformation is completed after 10,000 impacts. According to this assumption, coating fatigue takes place at a higher number of impact cycles. For this purpose, 10^4 and 10^6 impacts with different impact forces between 400 and 1,200 N were performed on each coated specimen of the DoE-run. Hereafter, the remaining imprint depth (RID) of the impact imprints were determined in terms of using confocal laser scanning microscopy (CLSM). The first step was the verification of suitability of the Bouzakis approach. In Fig. 25a and b measured profile lines of DoE-run 2 at 800 N and 1,000 N are presented after 10^4 and 10^6 impact cycles with representative impact craters. It can be seen, that the RIDs only differ minimal from each other at 800 N of impact force. At the opposite, the RID after 10^6 impact cycles tested with 1,000 N of impact force is significantly increased compared to $RID_{1,000\ N}(10^4)$. The increase in RID can be directly attributed to the coating fatigue, which is also evident from the corresponding impact crater. Dark areas are visible in the crater indicating erosive coating exposure which could be confirmed in SEM/EDX and CLSM analyses. With the equation of Bouzakis et al. taking the RIDs at different impact forces into account:

$$CFD_{force,i} = RID_{force,i}(10^6) - RID_{force,i}(10^4) \quad (5)$$

The force depended coating failure depth (CFD) was determined. Fig. 25c shows the different CFD curves for interpreting the impact resistance of the exemplary DoE-runs. As fatigue criterium a CFD value of 0.5 (black dotted horizontal line) was chosen which is linked to a complete fatigue of the functional a-C:H top layer of a thickness of 0.45 to 0.5 µm of all tested multi-layered coating systems. The CFD fatigue curves are characterized by completely different courses. The DoE-run 3 has the lowest whereas the DoE-run 2 is characterized by the highest fatigue resistance. No clear correlation to the hardness H_{IT}, toughness K or residual stresses $\sigma_{res.}$ was found for the exemplary present DoE-runs indicating that further coating properties are responsible for a low or increased impact fatigue resistance. For example, further influences can be attributed to the chemical coating composition and the associated binding states depending on the systematically set PVD process parameters. For this purpose, Glow Discharge Optical Emission Spectroscopy (GDOES) analyses were carried out at each DoE-run in order to study the chemical composition and the element depth profiles to the substrate interface. For example, the tungsten content can be correlated to the impact resistance.

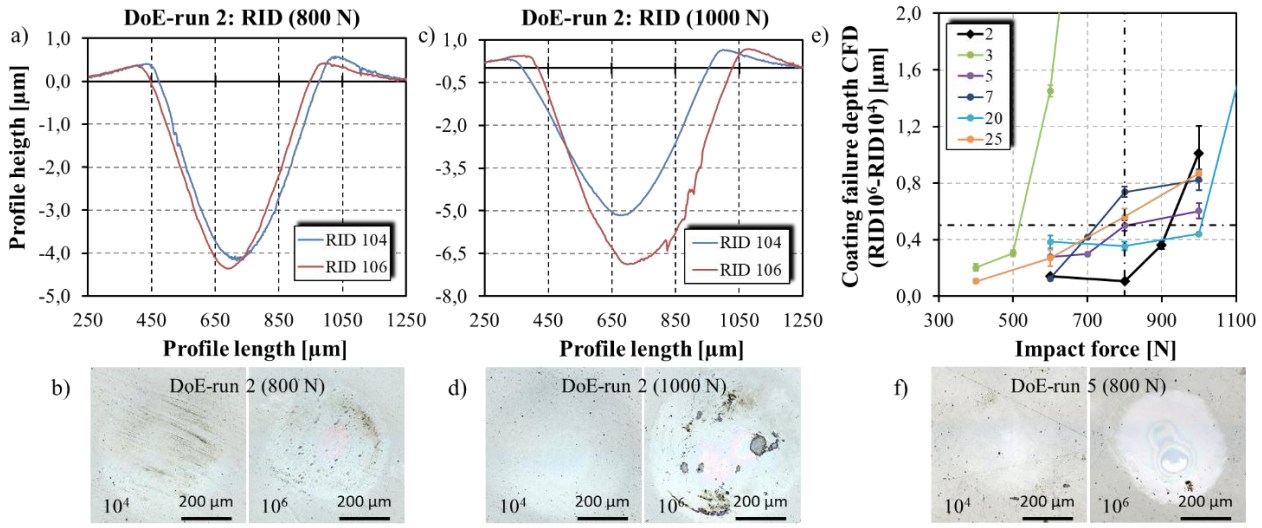

Fig. 25: Examples of: a) imprint profile lines of the DoE-run 2 at 800 N with b) corresponding impact craters after 10^4 and 10^6 impact cycles and c) imprint profile lines of the DoE-run 2 at 1,000 N with d) corresponding impact craters after 10^4 and 10^6 impact cycles for the calculation of the coating failure depth (CDF) curves for exemplary DoE-runs according to the approach of [76] and f) representative impact craters after 10^4 and 10^6 impact cycles of DoE-run 5 at 800 N impact force

The presented DoE-coatings of the CCI design were already applied on a newly developed single die set with further adjusted graded macrostructuring as a last evolution stage at the beginning of 2020. The die set should be investigated in order to systematically study the main influences of the coating properties compared to the performance in dry application testing. Unfortunately, due to the current situation caused by SARS-CoV-2 could not be tested conclusively yet

A promising possibility to improve the coating adhesion strength is nitriding of the steel prior to the PVD coating process. This DUPLEX treatment of nitriding and PVD coating process consists of the steps: quenching / tempering / plasma nitriding / coating. In this work the DUPLEX treatment was carried out at different N_2:H_2 gas flow rate ratios (6:43 l/h and 25:25 l/h) and plasma nitriding times (8 h, 25 h and 100 h). The flow rate ratios are denoted as 1:7 and 1:1 regarding the N_2 and H_2 gas conditions. After plasma nitriding, the half of specimen were subsequently polished (pol.) to 2 nm < Sa<12 nm and the other half of specimens were surface cleaned (cle.) without influencing the resulting roughness due to the nitriding parameters. Thus, a sample series of 12 different nitriding and surface states was available with one additional polished quenched and tempered reference which were all coated with the same coating system $DLC_{ref.}$ [77, 78].

Fig. 26 shows the resulting microstructures, the hardness profiles and critical loads Lc2 and Lc3 depending on the gas flow ratios 1:7 and 1:1 and surface conditions (pol.) and (cle.) of the most promising nitriding duration of 25 h [77, 78]. A ratio of 1:1 leads to the formation of a brittle compound layer (CL), see Fig. 26a. Furthermore, the diffusion layer (DL) is deeper compared to the gas ratio of 1:7 which can be explained by effusion-reducing effect of CL. Due to this effect, both the surface hardness $HV_{0.5}$ is higher and the hardness depth profile is shifted to a higher surface distance, see Fig. 26b. In Fig. 26c the scratch test results Lc2 and Lc3 are compared with the polished reference (Ref. pol.). Furthermore, the polished specimen with the coating system DoE-run 7 is included. It can be seen that both subsequently cleaned surface conditions achieve significantly

higher Lc2 than the polished surface states. Compared to Ref. pol. the increase is about three times higher indicating an increase of tolerance due to local overloading.

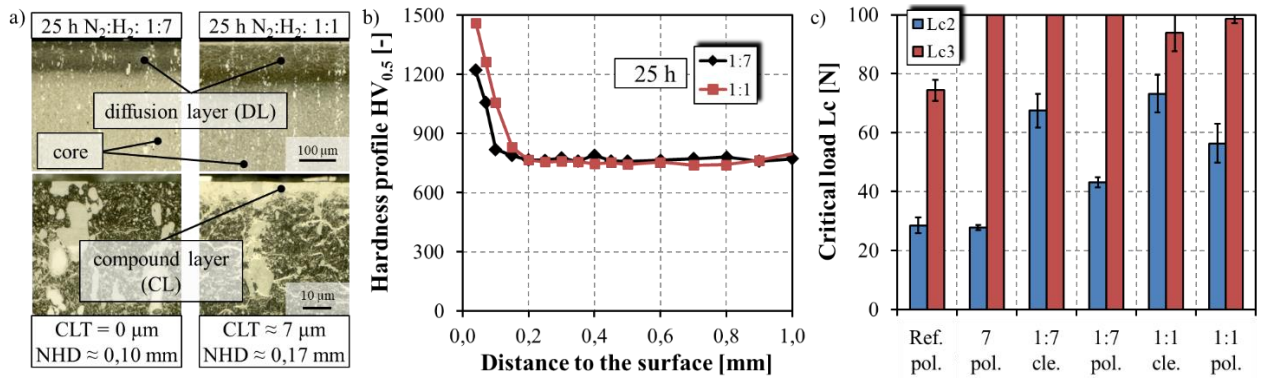

Fig. 26: Results of 25 h plasma nitriding: a) microstructures, b) hardness $HV_{0.5}$ profiles and c) critical loads Lc2 and Lc3 by scratch testing depending on the gas flow rate ratios 1:7 and 1:1 (N2:H2 l/h) and surface conditions polished (pol.) and cleaned (cle.) [77, 78]

3.5 Application testing of structured, coated and functionalized rotary swaging dies

3.5.1 Back motion and workpiece quality

All application tests were performed under lubricated (wet) and unlubricated (dry) conditions. At first, four die sets were tested which differ in unstructured and structured reduction zones as well as uncoated and coated forming zones after hard-milling, see Fig. 27. All sets exhibit the same basic die geometry, e.g. a die angle of $\alpha = 10$ °. Fig. 27a shows a conventional, i.e. commercial die with a thermally sprayed WC-Co coating, b and c show uncoated dies which differ in terms of a plane "smooth" and "structured" reduction zone ($\lambda = 1.3$ mm; $A = 0.15$ mm). Fig. 27d and e show coated dies with "smooth coated" and "structured coated" reduction zones ($\lambda = 1.3$ mm; $A = 0.15$ mm). These die sets exhibit an applied PVD a-C:H:W/a-C:H coating system already described above.

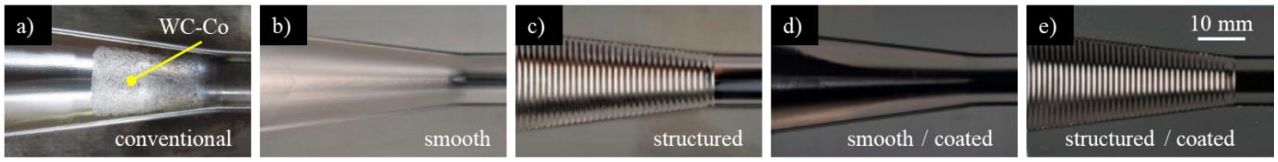

Fig. 27: Reduction zones of different die sets: a) conventional, b) smooth, c) structured, d) smooth and coated and e) structured and coated.

Fig. 28 shows the results for the back motion Δx at the highest feed rate of 2,000 mm/min for lubricated and dry rotary swaging of aluminum and steel tubes. At this experimental setup, the highest feed forces F_R, represented by the back motion, were determined for any die set [79]. The variants marked with a colored "X" could not be tested or tested only once due to immediate die failure. The highest back motion occurred for smooth and smooth coated dies for both materials at both lubrication states. The die sets with additionally applied macrostructuring exhibits the lowest Δx. The smaller back motion for AlMgSi0.5 workpiece material is due to lower material strength compared to S235, see Fig. 28a. Dry testing with conventional and smooth dies were aborted due process instability caused by excessive cold welding on the die surfaces. Dry testing with uncoated structured die sets had to be stopped after the first tube due to cold welding as well which explains the absence of the standard deviation bar. When forming steel with the structured coated dies the experiments were stopped, because macroscopic delaminations of the coating were observed, see Fig. 28b.

These results allow for several conclusions. Firstly, the axial reaction force F_R, can be significantly reduced by macrostructuring the reduction zone of the die. Secondly, the application of a-C:H:W/a-C:H coatings increases F_R. From this, it can be deduced that a functionalization and the related process control is possible in principle. Thirdly, coating of the dies actively reduces adhesion, enabling dry forming of aluminum at all.

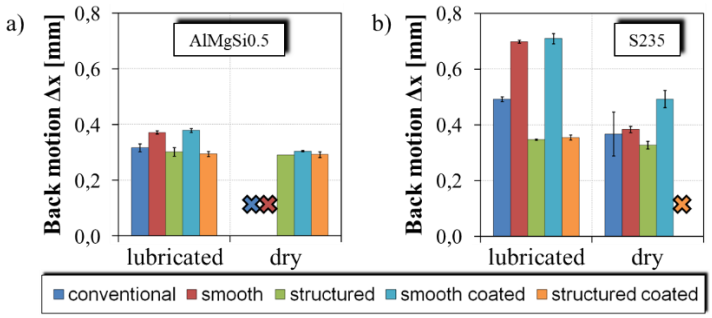

Fig. 28: Back motion Δx depending on the tested die sets and the lubrication state during rotary swaging for a) aluminum AlMgSi0.5 (3.3206) and b) structural steel S235 (1.0038) tubes at the highest feed rate of vf = 2,000 mm/min

After lubricated and dry rotary swaging, the resulting workpiece quality was analyzed for each die set. The measured deviation of roundness Ront and the arithmetic mean surface roughness Sa are shown for the highest feed rate of 2,000 min/min in Fig. 29. The variants with the colored crosses could not be tested for the reasons mentioned above. Fig. 29a and c represent Ront and Sa for AlMgSi0.5 tubes. Regardless of the lubrication state the lowest overall workpiece quality was obtained with structured (uncoated and coated) die sets which is probably the result of critical local contact conditions between die and workpiece along the structured reduction zone to the transition into the calibration zone. For smooth coated dies Ront increased approx. 220% for dry rotary swaging compared to lubricated conditions. The expected roundness deviation of the AlMgSi0.5 tubes dry formed by conventional and smooth dies should be significantly worse than using smooth coated dies. At the opposite, the roughness Sa after dry testing with smooth coated dies is in the range of conventional lubricated rotary swaging or even better. However, no dry rotary swaging was possible for conventional and also for uncoated smooth dies due to extreme cold welding and process instability. A direct comparison between the functionalized dies and reference is not possible for dry conditions due to the mentioned reasons.

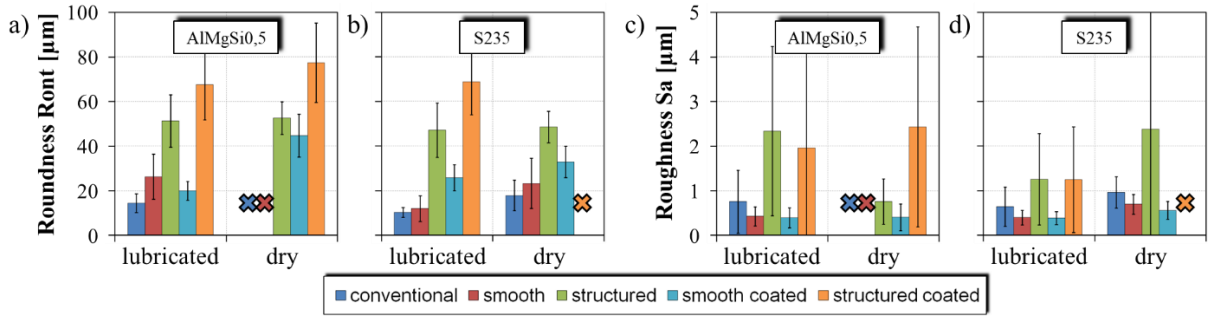

Fig. 29: Resulting workpiece quality after lubricated and dry rotary swaging at the highest feed rate (v_f = 2,000 mm/min): a) roundness deviation Ront of AlMgSi0, b) Ront of S235, c) surface roughness Sa AlMgSi0 and d) Sa of S235.

Fig. 29b and d show Ront and Sa for the S235 tubes. As already stated for the aluminum tubes, rotary swaging of structured (uncoated and coated) dies leads to high deviations of the roundness Ront. The best roundness results for dry rotary swaging were achieved using conventional and smooth uncoated dies. It became worse for smooth coated dies. Ront deteriorates of about 75 % for conventional dies when changing from lubricated to dry test conditions. Regarding the surface roughness Sa, the use of conventional dies leads to a deterioration of about 50 % due to the change to dry conditions. When the smooth coated dies are used, the deterioration is at least 45 %. However, it is remarkable that a better roughness Sa could be achieved when dry rotary swaging with smooth coated dies than with conventional dies under lubricated conditions which indicate the overall reference.

Intermediate conclusions: Structured dies reduce the back motion Δx respectively the feed force of the workpiece as desired and low friction hard coatings are indispensable for a successful dry rotary swaging of aluminum workpieces. With regard to the achievable workpiece quality after dry forming, it is obvious that there is still a challenge for improving the roundness, but the surface roughness is already improved compare to conventional lubricated rotary swaging.

3.5.2 Wear analyses

Wear analyses were carried out on the smooth coated and structured coated die using scanning electron microscopy (SEM) and energy dispersive X-ray spectroscopy (EDX).

Fig. 30 shows SEM pictures of the reduction (I), calibration (II) and the transition zones (I + II) of the smooth coated dies after dry rotary swaging of AlMgSi0.5 tubes. F_f indicates the feed direction of the workpiece material into the forming zone. The reduction zone exhibits extensive adhesion of aluminum primary localized at the tips along the feed marks due to the hard-milling process, see Fig. 30a. In the entire forming zone neither coating delamination nor smaller defects at high SEM magnification could be determined. Compared to the reduction zone, no appreciable aluminum cold welding is detected in the calibration zone, see Fig. 30b. The detected aluminum adhesions are locally concentrated at the milling grooves.

When forming steel tubes, different wear patterns are observed. No iron adhesion was detected by EDX in the entire forming zone. Small coating defects, localized at the tips along the milling feed marks occur in the reduction zone and are visible as white dots in Fig. 30c and in higher magnification in Fig. 30d. The dark particles localized at the white coating defects were found to contain the elements zinc, phosphorus and oxygen, indicating that these particles are zinc-phosphate particles coming from the phosphate corrosion protection of the steel tubes. The transition zone (from I to II) is characterized by beginning of abrasive wear, seen as bright areas on the left side of the vertical dotted line in Fig. 30e. These bright areas in the SEM-BSE image are due to back scattered electrons from the heavy tungsten atoms in the a-C:H:W layer. (The tungsten-free unworn a-C:H top layer appears darker in the SEM-BSE image [62].)

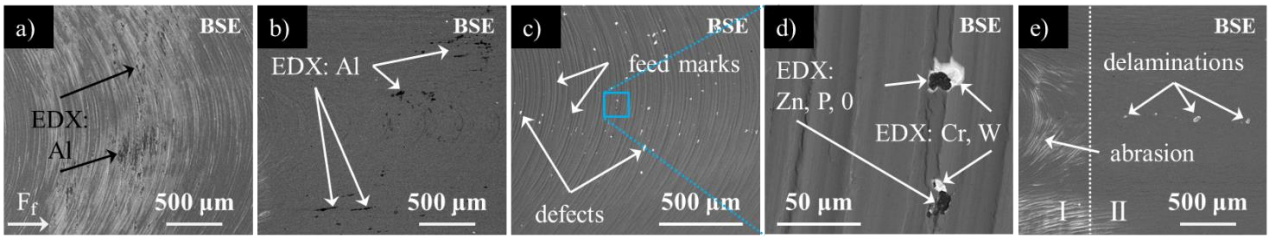

Fig. 30: Back scattered electron (BSE) SEM images of smooth coated dies: a) at the reduction zone (I) b) and at the calibration zone (II) after dry rotary swaging of AlMgSi0.5 tubes, c) at the reduction zone (I) and d) at higher magnification (blue box in c) and e) at transition zone (I and II) after dry rotary swaging of steel S235 tubes [62]

Fig. 31 illustrates the wear analyses of the structured coated dies after lubricated and dry rotary swaging of aluminum and steel tubes. When forming aluminum tubes, no coating defects could be observed by SEM at lower magnification in Fig. 31a. Only at a higher magnification beginning coating defects are detected in Fig. 31b showing two valleys and a summit of the macrostructure. Black vertical lines and adjacent white dots are visible in the valleys down to the flanks. The black lines show EDX aluminum signals indicating aluminum adhesion localized at the pronounced feed marks due to the hard-milling process. But these aluminum adhesions are much less pronounced compared to that at the smooth coated die in Fig. 30a. The white dots were identified as coating defects. No coating delaminations were observed in the valleys. However, the layer defects show increased tungsten signals, implying exposed a-C:H:W layers where aluminum preferably adheres. These results are in a good agreement with the results of dry pin-on-disc tests [62]. On the other hand, the summits of the macrostructure show first small coating delaminations, seen as larger white dots in in Fig. 31b and in Fig. 31c in higher magnification. Small spalling of the coating is visible on the summit. The spalling proceeds down to the hardened cold working die steel (1.2379). The more pronounced the topography of the feed marks, the larger the area of the coating defects and the more aluminum adheres at the coating. Due to the same milling processing in the calibration zone, the adhesion of aluminum on the surfaces is comparable to Fig. 30b. No coating defects or failures were observed in this zone.

Similar wear mechanisms were found after dry rotary swaging of the steel tubes. Severe coating delaminations occur at the summits of the macro-structure in the reduction zone, as shown in Fig. 31d. The higher magnification of these delaminations in Fig. 31e represents a wear pattern comparable to Fig. 31b. However, the macro-structuring exhibits both coating delamination as well as zinc phosphate adhesions from the structural steel tubes. The main delamination is located at the summits, whereas main adhesion is located in the area of the flanks and valleys. When dry forming aluminum the delamination achieves dimensions of about 50 µm. On the other hand, a few 100 µm wide delaminations were found when dry forming steel. Unlike the partial located adhesions in Fig. 30d, the same zinc, phosphorus and oxide adhesions, determined by EDX analysis, exhibit an area wide spread characteristic. The feed marks appear less pronounced in the valleys what could be a possible reason for these increased adhesion phenomena. The higher material strength might be possible for the smoothing of the milling induced micro-roughness during dry forming. These observations have to be studied further in detail. It should be emphasized that no major layer damage could be found in the valleys.

However, it is difficult to differentiate the delamination more precisely. It is not possible to distinguish whether the coating system is dynamically fatigued or an insufficient adhesion strength between coating and substrate is responsible for premature damage.

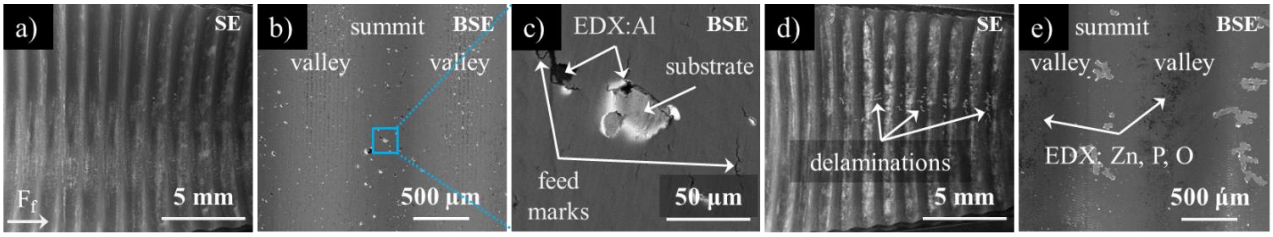

Fig. 31: Secondary electron (SE) and BSE SEM images of structured coated dies: a) at the reduction zone (I) and b) at higher magnification with c) high magnified single delamination on a summit after dry forming of AlMgSi0.5 (3.3206); d) at the reduction zone (I) and with e) higher magnification after forming of S235 (1.0038), cf. [62]

Intermediate conclusions: The wear analysis reveals that the macrostructure has to be designed more conservatively to avoid premature macro delamination by demands of the hard PVD a-C:H:W/a-C:H coating system; further, the transition from the reduction zone to the calibration zone should be designed in such a manner that the contact area between dies and workpiece in feed direction is increased [49, 62]. Also, the coating adhesion strength to the cold working steel should be increased.

3.5.3 Dies with advanced functionalization

Based on the results of the wear analyses, advanced functional rotary swaging die sets were developed, manufactured and tested. The following die types were investigated: smooth coated dies (smooth coated); uncoated and coated dies with a sine structure with lower amplitude (A = 0.05 mm, λ = 1.3 mm) (structured, structured coated); highly polished (Sa ≈ 20 nm) and smooth coated dies (polished coated); uncoated and coated dies with graded sine structure (graded structured; graded structured coated). The reduction zones of these different dies are shown in Fig. 32a to e.

Fig. 32f shows the measured back motions Δx of the feeding system at the highest feed velocity of 2,000 mm/min during lubricated and dry rotary swaging of S235 steel tubes. For lubricated rotary swaging, the unstructured dies show the highest back motion, the graded structured dies result in a significantly lower back motion and the structured and coated dies show the lowest back motion [64]. Dry rotary swaging was impossible for structured coated die due to early coating failure [49]. However, the degree of coating failure on graded structured and coated dies is not considered to be critical. Contrary to expectations, the very low back motion during dry rotary swaging with the polished coated dies is striking. This could be explained by the fact that the low surface roughness results in a high true contact area between tool and workpiece, which promotes adhesion and thus causes less back motion [49, 62].

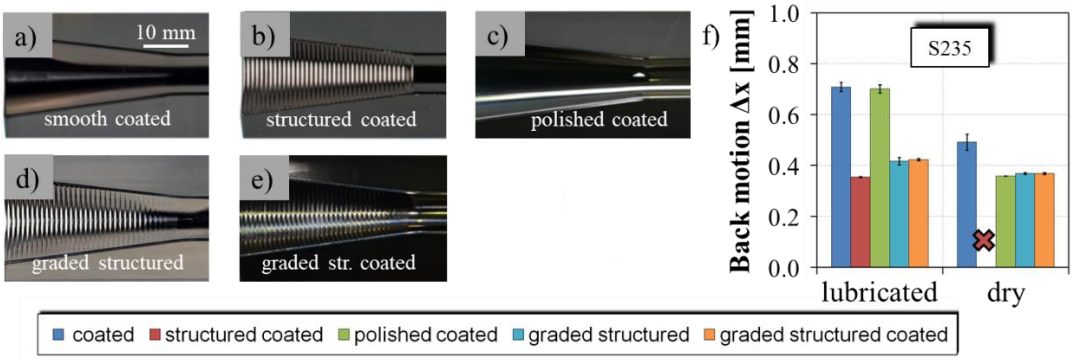

Fig. 32: Different rotary swaging dies: a) coated, b) structured coated, c) polished coated, d) graded structured, e) graded structured coated and f) back motion of steel forming with and without lubricant at v_f = 2,000 mm/min.

The workpiece quality of these advanced dies was analyzed, see Fig. 33. For forming of steel, it can be seen that graded structured dies allow an improvement in roundness and roughness compared to rotary swaging with dies with constant amplitude for lubricated and dry rotary swaging [64]. The comparison of coated and polished coated dies shows that fully polished functional surfaces of the dies cause increased roughness of the workpieces [62]. All the effects mentioned above occur similarly during rotary swaging of aluminum workpieces. Here too, grading the structure on the die allows for improved workpiece quality. However, the workpiece quality is lower compared to conventional dies.

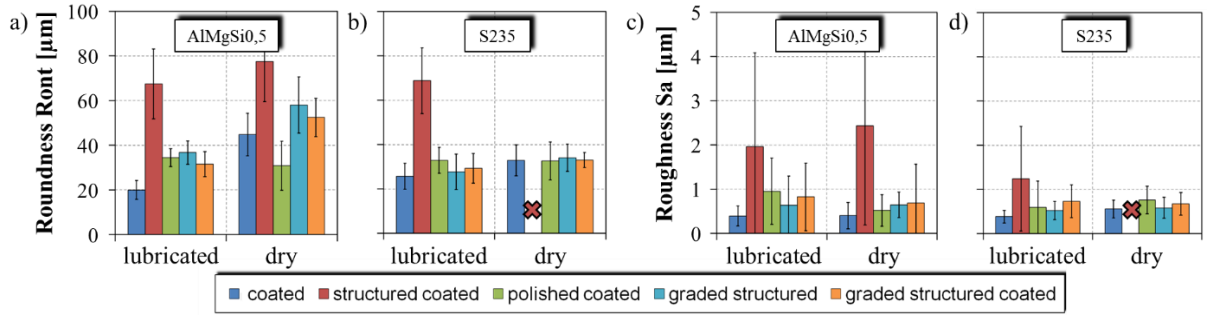

Fig. 33: Workpiece quality after rotary swaging (v_f = 2,000 mm/min) with different dies: a) roundness deviation Ront of AlMgSi0, b) Ront of S235, c) surface roughness Sa AlMgSi0 and d) Sa of S235.

A comparison of the axial process forces during the forming of steel tubes with differently structured die sets with the results from the simulation shows a good agreement. The axial process forces are normalized to the highest occurring value. It is shown that µ = 0.1 corresponds to the lubricated and µ = 0.2 to the unlubricated process. Accordingly, three differently structured die sets can be compared from the experiments: conventional dies without tungsten carbide-cobalt coating with a structure value of S = 0 µm, graded structured dies with S = 225 µm and constant structured dies with S = 400 µm, see Fig. 34. It turns out that for both lubrication conditions the development of the axial process force is well matched by the increase in the structure value. Only for the structure value S = 225 µm in the non-lubricated condition is a somewhat larger deviation observed, which can be attributed, for example, to changed stroke following angles, i.e. the relative angle between workpiece and dies rotation, at dry condition, which is not taken into account in the FEM.

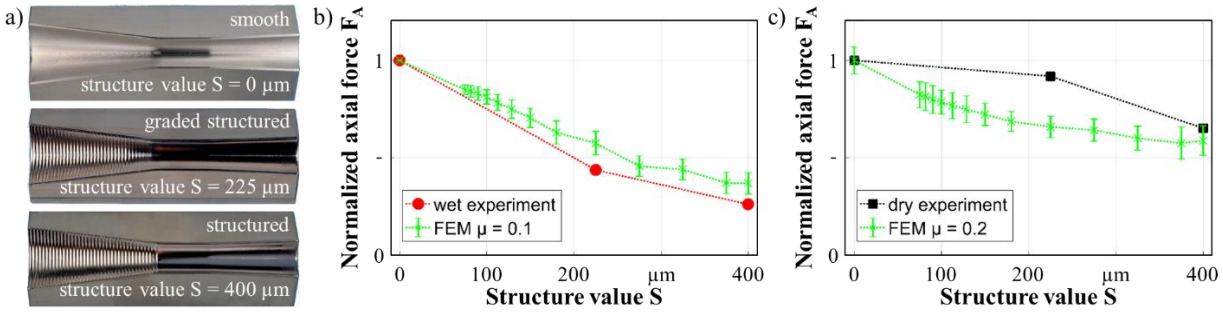

Fig. 34: Three differently structured dies: a) illustration of the die with different structure value S, b) normalized axial forces for lubricated forming and c) normalized axial forces for dry forming

Intermediate conclusions: Graded structures lead to an increase of the back motion, but at the same time to a significant improvement of the workpiece quality. Rotary swaging with polished and coated dies generally has a negative effect on the workpiece quality. Thus, a defined roughness helps to achieve a better workpiece quality.

3.5.4 Wear analyses of advanced dies

On the basis of the preceding wear investigations, initial measures for increasing the adhesive strength and fatigue resistance of functionalized rotary swaging dies were developed. Firstly, the influence of a preceding polishing process of the forming zone of non-structured dies was investigated. Fig. 35 shows the SEM images of the reduction and calibration zone after dry rotary swaging of aluminum and steel tubes.

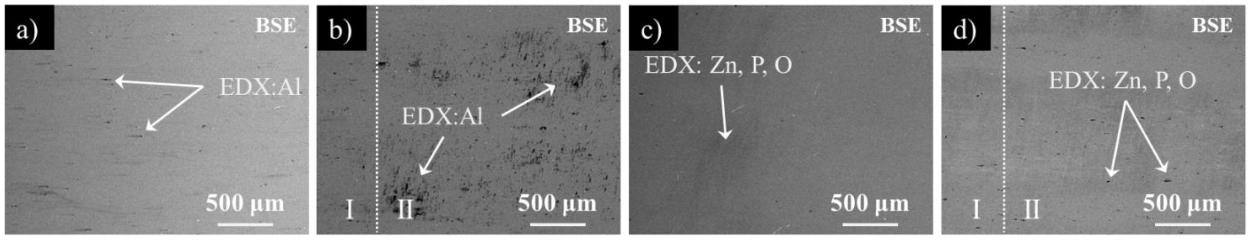

Fig. 35: BSE/SEM images of coated polished dies: a) reduction zone and b) corresponding transition zone after dry rotary swaging of aluminum tubes, c) reduction zone and d) corresponding transition zone after rotary swaging of steel tubes, cf. [62]

The examination of the forming zone proves that layer delamination no longer occurs. In comparison to the smooth, hard-finished dies, a contrasting adhesion appearance is shown. While finely distributed, locally limited aluminum adhesions are found in the reduction zone, see Fig. 35a, the adhesive wear in the calibration zone is much more pronounced and more extensive, see Fig. 35b. After forming steel tubes, laminar adhesion of zinc phosphates in the reduction zone occurred, and thus in the area of initial contact with the workpiece, see Fig. 35c. In the calibration zone, these zinc phosphates occurred as locally limited adhesion coatings, see Fig. 35d. In direct comparison to the smooth dies without polishing, the adhesion of both workpiece materials is lower in the reduction zone, but higher in the calibration zone. This allows two conclusions: Firstly, polishing of the reduction zone improves the adhesion strength to the substrate with regard to the macrostructure. Secondly, a specific surface finish in the calibration zone reduces adhesive wear or cold welding, which allows to improve the workpiece quality [62].

The following investigations show the wear behavior of the advanced coating in combination with the advanced macro structuring with graded amplitudes. Fig. 36 shows SEM images of the structured dies with constant and graded structuring after dry swaging of aluminum and steel tubes. The comparison of both amplitudes shows that the amount of layer wear and adhesion phenomena could be significantly reduced, see Fig. 36a and b. Only the wave where the initial contact between die and workpiece takes place (wave 7 and 8) shows layer delamination, see Fig. 36c. At the transition zone, no wear can be detected, in the calibration zone no adhesions could be detected. However, a minimal abrasive wear on the flanks (light-colored surfaces) is evident, see Fig. 36d. In the entire reduction zone, layer delamination could only be detected at a single point on the rotary swaging die under investigation. In general, abrasive and adhesive wear can still be detected in areas with clear milling marks from hard fine machining, see Fig. 36c and e.

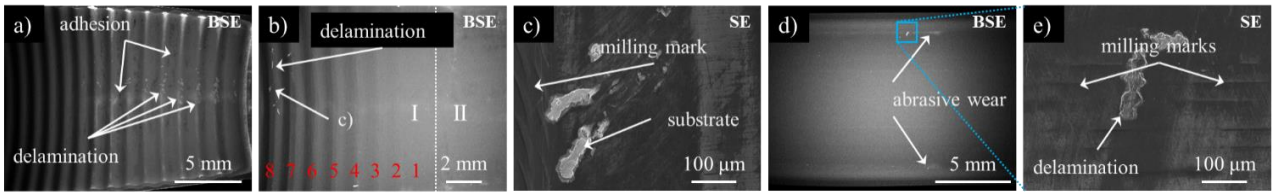

Fig. 36: BSE/SE/SEM images of different coated dies: a) constant amplitude and b) graded amplitude in the reduction zone, c) delamination at the eighth wave in first contact, d) calibration zone after rotary swaging with aluminum and steel and e) magnification of a single delamination

Fig. 37a shows a laser confocal microscopic measurement of a coated and polished surface. The profile section shows that growth defects of the a-C:H:W/a-C:H coating can have a height of up to one micrometer. On the one hand, these are located in the area of milling marks of the hard-fine machining process and on the other hand allow the explanation of the locally pronounced Al as well as Zn, P, O adherence even in the highly polished smooth dies. Based on the findings of the wear investigations and the size of the growth defects, a damage theory can be derived, see Fig. 37b. Here, layer defects and/or milling marks act as natural seeding points for incoming workpiece material which, as the forming process progresses, successively leads to cold welding and consequently to a critical contact situation. Local shear stress overloads of the layer can lead to layer delamination [80].

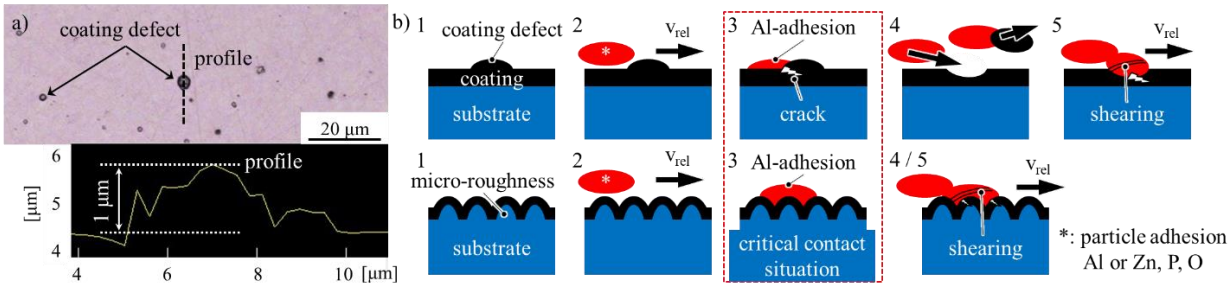

Fig. 37: Coating damage mechanisms: a) Laser confocal microscope image of polished surface with coating defect and b) damage theory of the coating based on the findings of the application test, cf. [80]

In order to study the effects on the DUPLEX treatment and the surface finishing a set of rotary swaging dies with graded amplitudes in the reduction zone according Fig. 36b was prepared for application testing. A quenched and tempered die was coated with the reference coating system from section 3.4 ($DLC_{ref.}$) and another die of the same heat treatment with the coating system of DoE-run 7, compare Fig. 21a. Due to the promising scratch test results of the subsequently cleaned DUPLEX treated surfaces of Fig. 26c two DUPLEX

treated dies with varied gas flow ratios N_2:H_2 (1:7 and 1:1) without and with a brittle compound layer and with no further surface finishing were tested with the applied DLC_{ref} coating system.

Fig. 38 shows the wear results in terms of an SEM/EDX analysis after a complete application testing program regarding the feed velocities of Fig. 6b for the four graded swaging dies differing heat treatment and surface states [80]. It can be seen, that the change in the target configuration from a WC to a pure W target can have a positive effect on the coating failure. The amount of coating defects and ZnP adhesions in the reduction zone could be reduced for DoE-run 7. While $DLC_{ref.}$ exhibits pronounced delaminations in the calibration zone, neither adhesions phenomena nor critical delaminations could be observed for DoE-run 7. This result could be linked to the high critical load Lc3 compared to $DLC_{ref.}$ of above 100 N while Lc2 is equal at 30 N. Furthermore, the both plasma nitriding variants with applied $DLC_{ref.}$ are free of coating defects or ZnP adhesion phenomena indicating the high potential for successful dry rotary swaging in long-term use [80]. In the calibration zone of the DUPLEX variant with a gas flow ratio of 1:1 one single delamination was determined. Detailed investigations under higher magnifications have shown that the substrate has also suffered a spallation within the brittle compound layer (CL). This result confirms the brittle behavior of the compound layers and indicates the DUPLEX treatment variant with a gas ratio of 1:7 as most promising for long-term tests.

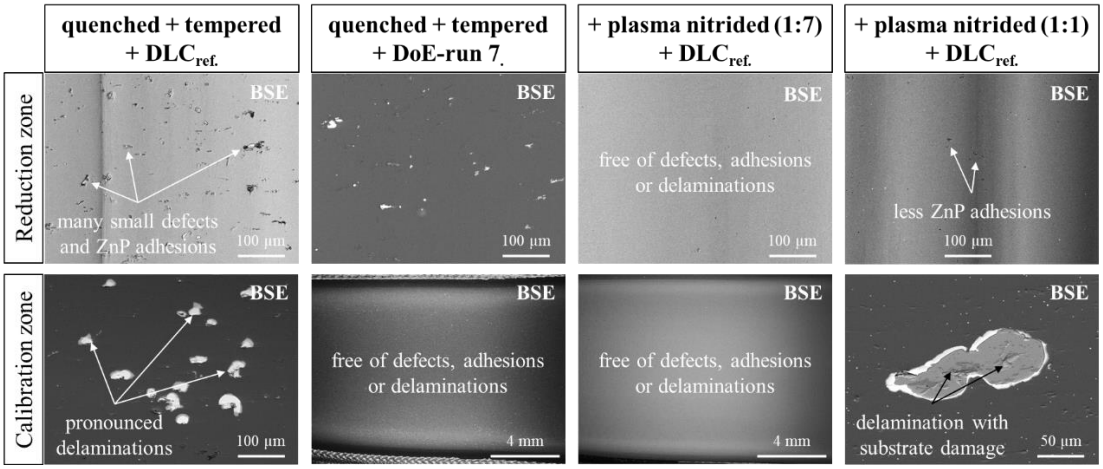

Fig. 38: Wear results of the different graded rotary swaging dies conditions after lubricated and dry testing according to Fig. 12b with different feed velocities 500 to 2,000 mm/min

Intermediate conclusions: The latter investigations reveal that a previously polished surface is advantageous for the adhesion of the coating to the substrate. A micro textured surface, on the other hand, shows advantages in terms of adhesive wear (cold welding), especially for the dry forming of aluminum, which also has a direct influence on the workpiece quality. Therefore, the surface should be polished in the reduction area where a high adhesion strength of the coating to the substrate is required, whereas the calibration zone should have a micro textured surface to avoid adhesive wear and to guarantee a sufficient workpiece quality. A DUPLEX treatment significantly increases the wear resistance of the applied a-C:H:W/a-C:H coating systems. For dry rotary swaging no further surface finishing is necessary subsequent to the plasma nitriding process. The variant with the compound layer (1:1) shows an equally good wear pattern compared to the plasma nitrided variant without compound layer (1:7). Nevertheless, the compound layer reacts critically to the impact and tangential load and shout not be used for dry rotary swaging dies.

3.5.5 Shape integrity of the structuring in the reduction zone

Also shape integrity of the structuring in the reduction zone was examined. The residual deformations of the macrostructuring which were calculated by means of FE simulations are insignificant. Even after the application tests with structured die sets no obvious deformation or a failure of the macrostructuring could be observed on any of the tools used. Nevertheless, for a more detailed investigation regarding the deformation, comparative measurements at the same die surface position were performed by means of confocal laser scanning microscopy. For this purpose, the die surfaces were measured at the same magnification (20X) directly after the hard-milling process, after the PVD coating deposition and finally after lubricated and dry application testing. This approach allows for a complete area comparison with the hard-milled surface acting as reference.

The surface images were recorded in the area of first contact between die and workpiece at the seventh and eighth wave of the structure. The comparison of the surfaces took place with the software CloudCompare. The

surface comparison of two measurements fields was performed using the best-fit algorithm. Fig. 39 illustrates absolute x-distances between the hard-milled reference and after the coating deposition as well as after the lubricated and dry application testing. The workpiece feed direction is depicted as F_f. Compared to the reference the deposition of the a-C:H:W/a-C:H coating system suggests a slight increase of the entire surface roughness, see Fig. 39a. At the opposite, the overall roughness appears to be slightly smoothed comparing the reference surface with the surface after application testing. Apart from that, the overall roughness appears to be slightly smoothed after application testing, comparing the reference surface with the recorded surface after the lubricated and dry tests, see Fig. 39b. The area related evaluation of both measurements showed that approximately 70% of the total z deviations are in the range of about 0.0025 mm. Deviations due to the best-fit algorithm cannot be completely excluded. Thus, a significant change of deformation can be excluded.

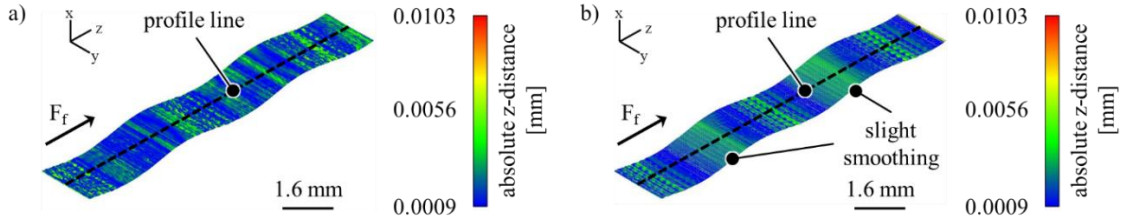

Fig. 39: Surface comparison at the same die position (7th and 8th amplitude) with the hard-milled surface used as reference: a) comparison between reference and after coating deposition and b) comparison between reference and after application testing of structured tools

For this reason, on each of the three surface measurements centered profile lines were exported, as it is exemplarily shown in Fig. 40. It can clearly be seen that the PVD deposition process slightly increases the roughness, especially at the left flanks at the first workpiece contact, compare hard-milled with coated in Fig. 40 (profiles are shifted vertically in the amplitude height for better visibility). After application testing with and without lubrication an overall smoothing of the micro-roughness is determined. An increased residual roughness is shown after the tests on the right flanks towards the valleys. This can also be an explanation for the increased tendency to adhesion of the workpiece material. In view of the investigations presented, plastic deformation of the macrostructure and its negative influence on the coating can be excluded.

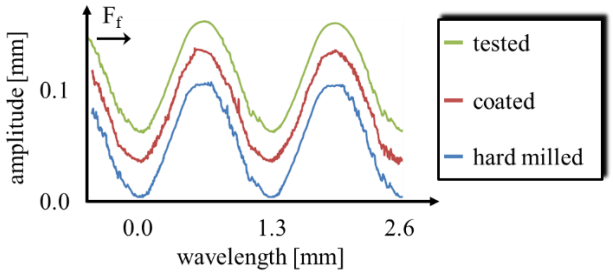

Fig. 40: Comparison of the centered profile lines in feeding direction on the structured die after hard-milling, PVD coating and application testing (profiles are shifted in the amplitude height for better visibility)

Intermediate conclusions: The amplitudes of the macrostructures in the area of first contact to the workpiece material were recorded by CLSM stitching with a scanning length of approx. 3.0 mm after hard-milling, coating deposition and after application testing. No plastic deformation on the critical positions of the macrostructures could be observed as a result of the applications testing. An overall surface smoothening on the macrostructures took place with exception in the right valley areas at the opposite side of the of the workpiece feeding. Here, a slight increase in surface roughness Sa was determined which correlates to the areas of increased cold welding.

3.6 Investigations on the macro- and microstructures

3.6.1 Investigations on the formation and movement of wear debris with macro-structured dies

Dry rotary swaging leads to an increased generation of wear debris detached from the workpiece material. Due to the lack of rinsing off the lubricant the wear debris cannot be removed sufficiently from the forming zone and the swaging unit, which can lead to a deterioration of the workpiece quality and a premature termination of the process. As a basis for the development of die-side adaptations to reduce particle generation and to increase the particle ejection from the forming zone, dry rotary swaging tests were performed and the resulting workpiece abrasion was characterized [57]. The functionalized rotary swaging dies used for this purpose had a reduction zone with a continuous sine structure ($A = 0.05$ mm, $\lambda = 1.3$ mm) and an additionally applied a-

C:H:W/a-C:H coating system. Workpieces made of aluminum alloy AlMgSi0.5 and the unalloyed structural steel S235 with and without zinc phosphate anti-corrosion coating were formed. Following to the individual experiments, the rotary swaging dies were removed from the swaging unit and the remaining wear debris from the reduction and calibration zone were rinsed into Petri dishes. In addition, particles that remained on the die flanks were collected. The characterization of the collected wear debris according to their areal expanse and quantity was carried out by light microscopy using the image analysis software Image Metrology SPIP.

The formation of wear debris during dry rotary swaging with functionalized dies is led back to the contact conditions between die and workpiece. Repeated compressing and stretching of the near-surface workpiece material on the sinusoidal structured die surfaces leads to strain hardening and finally to failure due to embrittlement. The material detaches from the workpiece in the form of tinsels. Due to the rotary motion of the swaging unit, a majority of the particles is transported into the gap between the single swaging dies, so that the largest accumulation of abrasive particles occurs here, regardless of the material being forged. The repeated opening and closing of the dies in the rotary swaging process also forms the particles into tinsels with a significantly larger areal expanse. In particular, the accumulation of particles on the die flanks can ultimately lead to premature failure of the dry rotary swaging process, by preventing a complete closing of the dies.

In addition to the investigations regarding the formation of wear debris, dry rotary swaging experiments were carried out with uncoated dies which had the same macrostructure in the reduction zone (A = 0.05 mm, λ = 1.3 mm). When rotary swaging aluminum workpieces at a high feed rate of 2,000 mm/min, a direct comparison with the results of the rotary swaging tests with coated dies revealed an up to tenfold higher amount of wear debris. Besides the tinsels generated had surface areas which were up to 500 % larger, see Fig. 41. The results of this experiment impressively underline the ability of the applied a-C:H:W/a-C:H hard coating system to suppress cold welding and the associated significantly increased generation of wear debris.

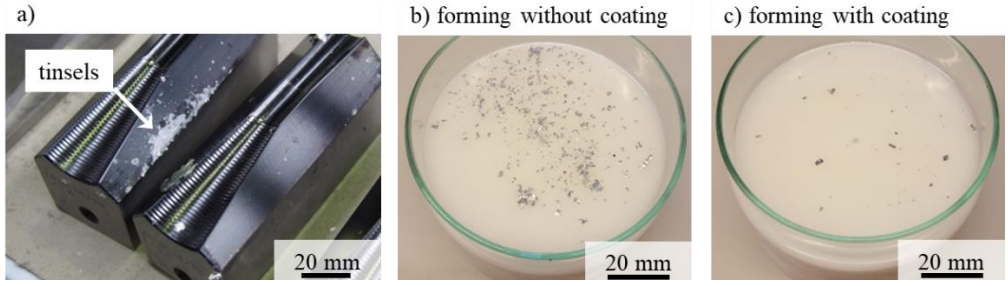

Fig. 41: a) Wear debris of AlMgSi0.5 collected from the tool dies after application testing at vf = 2,000 mm/min, b) wear debris with structured uncoated dies and c) wear debris with structured coated dies, cf. [57]

The reduction of wear debris formation during dry rotary swaging was achieved by adjusting the sinusoidal structure in the reduction zone. For this purpose, a graded structure with a continuously decreasing amplitude was tested. This type of macrostructure represents a good compromise between reduced wear debris formation and at the same time sufficient reduction of the axial reaction force and has been implemented for a set of functional rotary swaging dies. Fig. 42 shows Petri dishes with wear debris generated during rotary swaging with graded dies. It can be seen that the quantity of wear debris has decreased significantly [81].

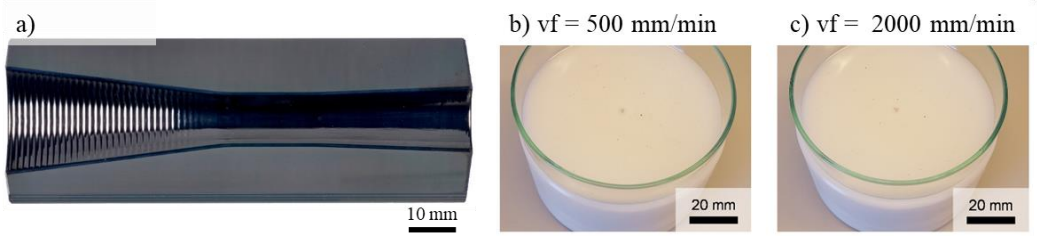

Fig. 42: Wear debris from aluminum rinsed from the reduction and calibration zone of coated graded structured dies after the experiments: a) coated graded structured die; b) petri dishes after forming with vf = 500 mm/min and c) petri dishes after forming with vf = 2,000 mm/min, cf. [81]

The motion behavior of wear debris on sinusoidal structured surfaces was investigated in tribological model experiments with multiple excitation [67]. Workpiece specimens made of AlMgSi0.5 and structural steel S235 were used for the investigations. Within the experiments wear debris, previously collected in dry rotary swaging tests, were applied to the die samples. Ten repetitive impacts (drop height h_d = 0.05 m, short-term surface pressure of 0.64 kN/mm^2) were carried out and the change in position of the wear debris on the die samples was documented photographically after each impact, see Fig. 43.

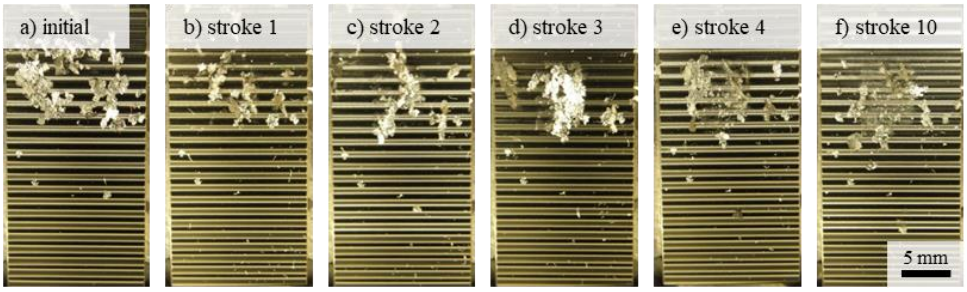

Fig. 43: Steel wear debris; a) applied on sine structured tool specimen (λ = 1.3 mm, A = 0.05 mm), change in position of the particles depending on the number of impacts applied in the tribological model test: b) to f)

All die samples investigated suppressed largely the movement of wear debris due to the applied impacts. This is explained by a sequence of summits and depressions of the structured surfaces transverse to the feed direction of the workpiece in the experimental setup. The observed behavior of the wear debris is associated with an extended remaining of the particles in the forming zone during rotary swaging and thus a deterioration of the workpiece quality. A slightly inclined arrangement of the sinusoidal structure should allow the movement of the wear debris while controlling the reaction force at the same time.

Intermediate conclusions: Sinusoidal macrostructures are able to control the axial reaction force. But they also cause the formation of wear debris, which have a negative influence on the process and the workpiece quality. The application of a-C:H:W/a-C:H coatings and an adjustment of the macrostructure from a continuous to a graded structure reduces the formation of wear debris immensely. Current investigations are focusing on a slight inclination of the macrostructures, in order to transport the low number of wear debris still being generated out of the forming zone.

3.6.2 Tribological model tests to study the adhesive wear of coated microstructures

To study the phenomenon of aluminum adhesive wear in the calibration zone of polished and coated rotary swaging dies, a special designed tribological test rig was used, see Fig. 15. The results are used to adjust the design of the macro- and microstructures of the surfaces in the calibration zone. For the tests, eight microstructured die samples were made from tool steel 1.2379. Four microstructures are exemplary shown in Fig. 44a, denoted as MS1 toMS4. The microstructuring was carried out by line-milling with ball end milling tools (variation of feed per tooth f_z, radial depth of cut a_e and tilt angle α), a procedure known from the manufacture of micro forming dies with tribologically effective surfaces [32]. The generated microstructures with arithmetical mean heights in a range of 140 nm < Sa < 866 nm differ significantly in the particular appearance of the topography. In addition, the surface near residual stresses δ_{res} were determined by X-ray diffraction (XRD) in milling as well as transverse to milling direction, see Fig. 44 b. Furthermore, a polished workpiece sample was produced as a reference with a surface roughness Sa = 10 nm. Considering Fig. 44 b, it seems that the progressions of roughness and residual stresses are in opposite directions. This can be explained by ploughing effects component in the milling process which varies for different milling parameters. A high amount of chip removal and in consequence a low ploughing leads to high surface roughness and a comparatively low residual stresses, as it can be observed for microstructure MS1. At the opposite, the surface roughness is low and the resulting residual surface stresses are high for the microstructure MS4 indicating a high ratio of ploughing during the milling operation. Furthermore, the milling tracks of the topography of microstructure MS4 appear interlocked, which also indicates that significant ploughing occurs. Thus, selecting the milling parameters the chip removal and amount of ploughing can be adjusted to control the intrinsic properties and the geometric characteristics of the microstructures.

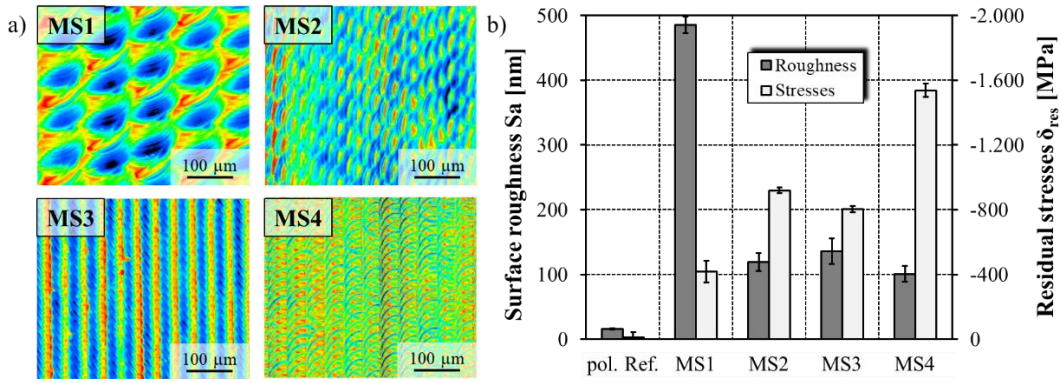

Fig. 44: a) CLSM topography images and b) Surface roughness Sa and surface near residual stresses δ_{res} of the die samples MS1 to MS4

Subsequent to the milling and analyzing, all die samples were coated with the coating system DoE-run 5, which is characterized by a high hardness, increased compressive stress and a sufficient adhesion strength to the substrate material.

The workpiece samples for the tribological rig tests were made of aluminum AlMgSi0.5. During the tests the impact surface pressure was set to 0.65 kN/mm^2 by adjusting the drop height of the excitation mass in the test rig. This impact pressure was about two times higher than the average surface pressure during rotary swaging in order to provoke cold welding of aluminum.

The test rig results show that the surface of the die samples has a decisive influence on the adhesive wear of aluminum. Fig. 45 shows SEM/BSE images of the polished reference (pol. Ref.) and the micro-milled topographies MS3 and MS1. (Aluminum adhesions appear dark in the BSE images.) Compared to the polished reference the amount of optically detectable adhesions could be decreased for topography MS1. The measuring fields 1-3 were used to quantify the aluminum adhesions occurring on the die samples.

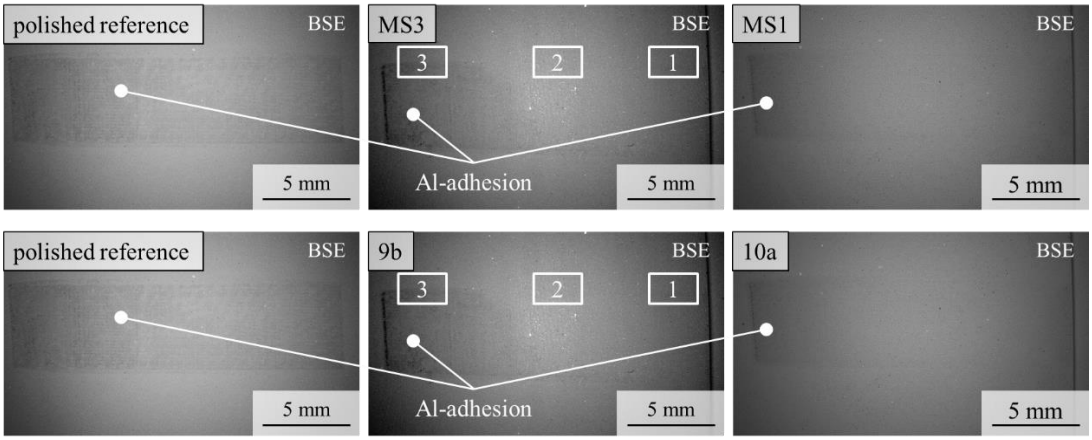

Fig. 45: SEM image (BSE) of the die samples: polished reference, 9b and 10a with aluminum adhesions

After one stroke on each of the die samples, SEM images were obtained for evaluation. The amount of adhesive wear was evaluated by automated image analysis. The BSE images were evaluated for their roughness dependent change in black percentage before and after the tribological testing, which subsequently could be addressed to the aluminum adhesions. The SE (secondary electrons) images were examined for their bright fraction, which allows for the determination of the relative area of delamination $A_{D,r,total}$ of the applied coating system DoE-run 5. For the evaluation of the adhesion, three smaller areas of the SEM image were evaluated at the same positions on all samples, see Fig. 45. The black and white conversion of the single fields are presented in Fig. 46 a. The functionality of the image analysis is explained in detail in section 3.4. Fig. 46 b shows the results of the image analysis regarding the adhesion increase and occurring delaminations. Depending on the microstructure the amount of adhesion could be significantly decreased compared to the polished reference. At the opposite, the delaminations $A_{D,r,total}$ increase for the tested microstructures. A probable explanation for the reduced adhesive wear can be linked to the junction growth theory. This theory describes that the real contact area between two friction partners (workpiece and die) increases under superimposed normal and tangential loads [82]. This increase in contact area is caused by the elasto-plastic deformations of the microcontacts of both partners and thus reduces the surface pressure, which leads to less adhesive wear.

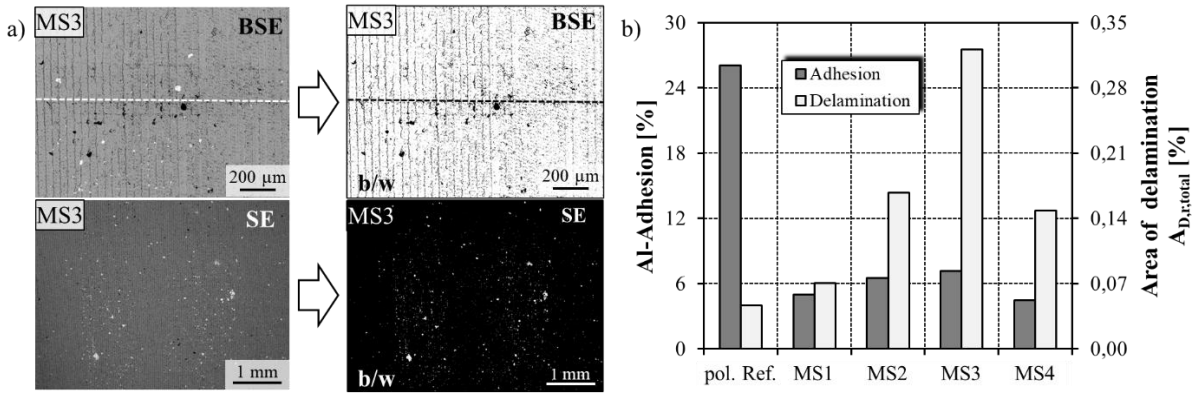

Fig. 46: a) SEM input image (BSE+SE) of the die sample MS3 with black and white conversion and b) Evaluated aluminum adhesion and determined area of delamination $A_{D,r,total}$ of the applied coating DoE-run 5

3.6.3 Impact tests to characterize fatigue of the coatings

The manufactured surface textures were coated with the coating system DoE-run 5, compare Fig. 21a, and subsequently tested with the impact tribometer. The described CFD method of Bouzakis et al. is not applicable due to the differences in surface roughness of the microstructures MS1 to MS4 [76]. For an approximation of the impact strength load increase impact tribometer tests were carried out between 200 N and 800 N with 10^4 cycles in order to study the beginning of adhesive coating delamination. It was found out, that first small delaminations occur above 600 N for all tested microstructures. For this reason, the specimens were tested at 800 N impact force with 10^5 cycles in order to provoke a determinable damage pattern. Fig. 47a represents procedure for analyzing the resulting impact craters for 800 N (10^5) of the determinable failed area ratio FR according to the works of Bouzakis et al. [83]. In a first step, the overall crater area CA is determined. Due to an image analysis process the failed area FA is determined. CA and FA can then be used to calculate F_R. In Fig. 47b and c the representative impact crater of the microstructures and the calculated failed area ratios FR are shown. FR is less than 5 % for the microstructures MS1 and MS2. The microstructures MS3 and MS4 show considerable failed area ratios between 10 and 25 %. A direct correlation between the roughness, residual stresses, Al adhesions and $A_{D,r,total}$ could not be found, However, with regard to the presented results the microstructure MS1 indicates an optimum for the application testing with micro-structured calibration zones.

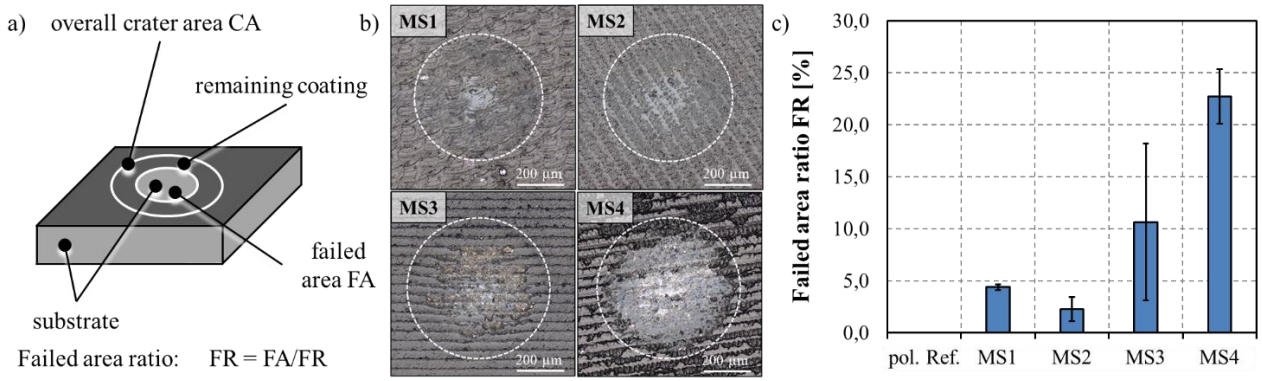

Fig. 47: Area impact crater analysis: a) procedure for determining the failed area ratio FR according to [83], b) representative impact craters and c) measured FR by image analysis of the microstructures 10a, 6b, 9b and 7a

3.6.4 Wear analysis on micro-structured dies

With regard to the results from the sections presented above, flat dies with three different microstructures in the calibration zone as well as one flat die with a polished calibration zone as a reference were manufactured in order to study the adhesive die wear when dry forming of aluminum tubes. For reasons of comparability, the investigations were carried out at a constant feed velocity of 500 mm/min. In addition, the lowest feed velocity leads to the highest amount of tool strokes, which results in a high amount of impacts between workpiece and die surfaces and thus forces the occurrence of cold welding.

Next to the polished reference (pol. Ref.) the microstructures MS1, MS3 and MS4 were coated with the coating system DoE-run 5, tested and subsequently analyzed. Thus, dry testing with one single tool set, allows considering the micro-milling related surface conditions as well as the adhesive wear with the coating fatigue properties, simultaneously in laboratory scale.

are presented. Fig. 48a shows the overview of the transition zone from the reduction into the completely presented calibration zone. For the micro-structured dies MS3 and MS4 wear phenomena took place within the white boxes located in the upper right area of the BSE images. No wear phenomena could be observed for the polished reference and the micro-structured die MS1 in this location. In Fig. 48b the indicated areas are presented as BSE image under higher magnification. Four different wear phenomena can be observed here. For the polished reference die a slightly detectable area of Al adhesion could be detected by EDX. For the micro-structured die MS1 no Al adhesions could be detected. However, the BSE image of the MS1 die exhibits small white dots which were identified as small coating defects by an increased tungsten peak in the EDX spectrum. The location of the defects can be linked to the highest position of the topography. A large white area is located in the center of the micro-structured die MS3. SEM/EDX analyses have revealed that these areas are cold welding as well as adhesive coating delaminations, which can be linked to the wear mechanisms presented in Fig. 37. For the micro-structured die MS4 the amount of Al adhesions ranges between MS1 and MS3. At the opposite, no adhesive coating delaminations could be determined. These results are in good agreement to the tribological tests rig results in Fig. 46b and can therefore be considered transferable for application testing. An influence on the surface roughness Sa and the surface near residual stresses $\sigma_{res.}$ could not be proven. On basis of the presented results it is concluded that non-graded microstructures (with constant amplitude) oriented normal to the feed direction are disadvantageous for dry rotary swaging.

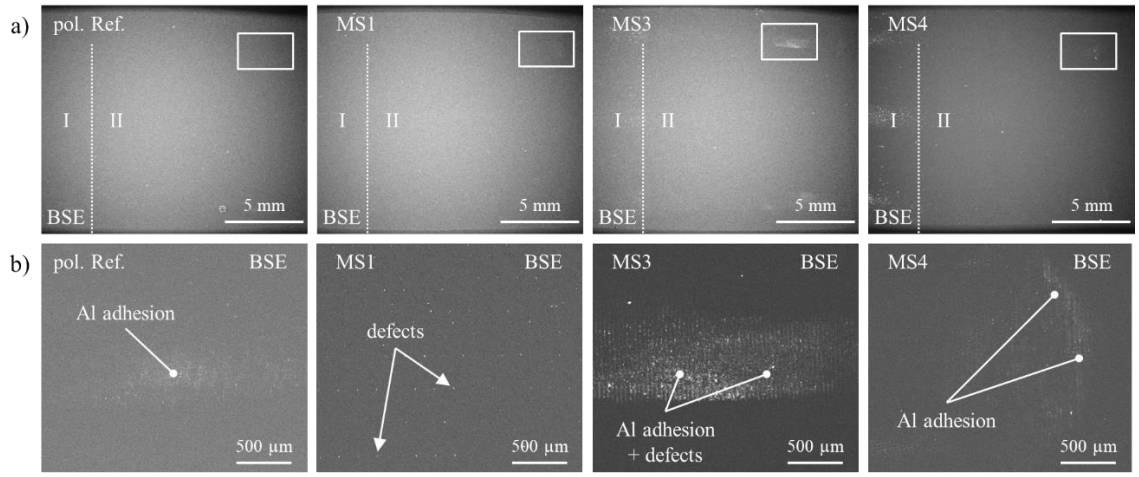

Fig. 48: Adhesive wear analysis on the micro-structured flat dies: SEM/BSE images of a) transition zone from reduction zone I to micro-structured calibration zone II and b) adhesive phenomena of the measuring field of (a) at higher magnification after dry forming of aluminum tubes

Intermediate conclusions: Different microstructures were tested at laboratory scale as well as in application testing. It could be demonstrated that a strong correlation between the developed tribological test rig and the adhesive wear results on flat dies in dry application testing exists. The type of microstructures applied by 5-axis hard-milling can be adapted to optimize the amount of delaminations and the tendency for cold welding of aluminum. No correlation could be found between the surface roughness Sa, the surface near residual stresses $\sigma_{res.}$ and the feasibility for application testing. Purely linear shaped structures are disadvantageous for application testing. It has been demonstrated that microstructures have a high potential to reduce adhesive wear. However, the surface topography and alignment of the structures have a decisive influence on the ability to minimize wear.

4 Conclusions

A rotary swaging process design for unlubricated (dry) conditions was developed by an interdisciplinary approach using modelling/simulation, mold manufacturing, coating, tribological testing and forming process technology. By structuring and coating functionalized dies are developed to fulfill all requirements for dry rotary swaging for two workpiece materials: a construction steel S235 (mat. no.: 1.0038) and an aluminum alloy (mat. no.: 3.3206). The parameters of the manufacturing processes and the achieved work piece quality, i.e. the geometry (roundness and surface) of the formed parts, are examined comprehensively. In the end, the

feasibility of dry forming is demonstrated and also the difficulties that arise. In detail the following conclusions can be drawn:

- Optimum friction conditions for low axial and radial process forces were identified by FEM simulations; a high effective friction in the reduction zone and a low friction in the calibration zone is desired.
- FEM simulations also revealed, that macro-structured dies with a constant sine shape in the reduction zone reduce the axial force with increasing amplitude, while the radial force is barely influenced. The structuring increases the effective friction which is experimentally confirmed by cylinder compression tests.
- The tribological test rig exhibited lower back pushing during an individual impact of a steel or aluminum workpiece specimen by a structured tool specimen which correlates well to the FEM simulations.
- Dry forming with conventional dies is not or just badly possible: dry forming of aluminum leads to extensive adhesion phenomena resulting in a premature conventional die destruction. By dry forming of steel, high amounts of abraded particles were found in the forming zone which negatively affects the workpiece quality
- Dry rotary swaging of aluminum and steel tubes leads to slightly higher process temperatures of still below 160 °C, mainly on the inner wall side of the tubes.
- The application of tungsten doped a-C:H coatings by reactive magnetron sputtering enables dry rotary swaging of steel and aluminum.
- The process temperatures determined have no effect on the degradation of the coating properties.
- The deposition of graded multi-layered Cr/CrN_x/a-C:H:W/a-C:H coating systems significantly reduced the coefficient of friction and the coefficients of wear of the counter body and coating in dry pin on disk tests
- The coating wear can be attributed to the wear resistance of the coated dies and the pin wear coefficient can be used as an indicator of the expected workpiece quality.
- The critical load Lc3 is an important parameter from scratch testing for dry rotary swaging in terms of the formed amount and size of coating delaminations.
- The application of Cr/CrN_x/a-C:H:W/a-C:H coatings have a major impact on the reduction of wear debris and adhesion phenomena in dry rotary swaging increasing the workpiece quality.
- In the case of a constant sine macro-structured reduction zone the workpiece quality – i.e. roundness deviation and surface roughness – are influenced in a negative way. The structure in the reduction zone needs to be graded and the design is to be interpreted conservatively to achieve a good workpiece quality.
- Especially the dry processing of steel causes coating delaminations due to cold hardening in the reduction zone of the die. Furthermore, a conservative grading and a subsequent polishing step of the macro-structure significantly enhances the coating adhesion.
- At the opposite, a super finished calibration zone favors the microscopic adhesion phenomena in the calibration zone reducing the workpiece surface quality. A fine microstructure is needed to control both, the adhesion phenomena and thus the workpiece quality. The micro-structuring has to be adapted to the applied PVD-coatings.
- A further improvement of the coating to reduce the delaminations during the dry processing is the DUPLEX treatment. A plasma nitrided surface without a compound layer in combination with an adapted coating system leads to no coating errors after forming aluminum and steel tubes.
- For a successful dry rotary swaging design for long-term use a combination of the following steps should be considered: quenching, tempering, application of a conservative graded sine macro-structuring in the reduction zone, application of an adapted micro-structuring in the calibration zone, plasma nitriding without a subsequent surface finish and deposition of an optimized multi-layered tungsten doped a-C:H coating system.
- An optimized tool set regarding the above-suggested process steps with a systematically developed coating system was already manufactured at the beginning of 2020, but due to the current situation caused by SARS-CoV-2 could not be tested conclusively yet.

In the end, it is shown that by combination of diamond-like-carbon coating of the complete forming zone and graded sine structuring of the reduction zone, functionalization of rotary swaging dies for a dry process design to process steel and aluminum tubes is successfully established. The extensive investigations also reveal that only an intense mutual research effort is leading to sufficient results for the successful development and finally implementation of a dry forming process, here dry rotary swaging. Only the combination of comprehensive theoretical (e.g. modelling and simulation) and experimental investigation as well as elaborated characterization methods enable to significantly proceed towards forming processes under dry conditions.

Acknowledgements

The authors gratefully acknowledge the Deutsche Forschungsgemeinschaft (German Research Foundation - DFG) for funding this work "Potentials of Dry Rotary Swaging" within the priority program "Dry metal forming - sustainable production through dry processing in metal forming" – DFG Grant No. KU1389/14; RI1108/5; ZO140/13 – 244812294.

References

[1] E. Rauschnabel, V. Schmidt: Modern applications of radial forging and swaging in the automotive industry, Journal of Materials Processing Technology 35 (1992) 371–383.
[2] S.-J. Lim, H.-J. Choi, C.-H. Lee: Forming characteristics of tubular product through the rotary swaging process, Journal of Materials Processing Technology 209 (2009) 283–288.
[3] V. Piwek, B. Kuhfuss, E. Moumi, M. Hork: Light weight design of rotary swaged components and optimization of the swaging process, Int J Mater Form 3 (2010) 845–848.
[4] H. Alkhazraji, E. El-Danaf, M. Wollmann, L. Wagner: Microstructure, Mechanical, and Fatigue Strength of Ti-54M Processed by Rotary Swaging, Journal of Materials Engineering and Performance (2015).
[5] S.J. Lim, H.J. Choi, K.H. Na, C.H. Lee: Dimensional Characteristics of Products Using Rotary Swaging Machine with Four-Dies, SSP 124-126 (2007) 1645–1648.
[6] S.A. Najafabady, A. Ghaei: An experimental study on dimensional accuracy, surface quality, and hardness of Ti-6Al-4 V titaniumalloy sheet in hot incremental forming, Int J Adv Manuf Technol 87 (2016) 3579–3588.
[7] H.-F. Wang, J.-T. Han, Q.-L. Hao: Influence of Mandrel on the Performance of Titanium Tube with Cold Rotary Swaging, Materials and Manufacturing Processes 30 (2015) 1251–1255.
[8] B. Kuhfuß: Hollow drive shafts - a contribution towards weight and cost reduction in automotive construction, Automotive Technology International (1998).
[9] F. Vollertsen, F. Schmidt: Dry metal forming: Definition, chances and challenges, Int. J. of Precis. Eng. and Manuf.-Green Tech. 1 (2014) 59–62.
[10] R.L. Kegg: Mechanics of the Rotary Swaging Process, Journal of Engineering for Industry 86 (1964) 317.
[11] R. Haug: Rundkneten im Vorschubverfahren. Zugl.: Stuttgart, Univ., Diss.,, DGM-Informationsges. Verl., Oberursel, 1996.
[12] M. Krüssmann: Rundkneten im Einstechverfahren: Prozessanalyse. Zugl.: Stuttgart, Univ., Diss.,, DGM-Informationsges. Verl., Oberursel, 1996.
[13] F. Müller: Verfahrensgrundlagen des Rundknetens. Zugl.: Darmstadt, Techn. Hochsch., Diss., 1997, Als Ms. gedr, Shaker, Aachen, 1997.
[14] R. Gärtner: Entwicklung einer optimierten Fertigungsstrategie für das Kaltrundkneten, Diss. TU Darmstadt (1999).
[15] A. Ameli, M.R. Movahhedy: A parametric study on residual stresses and forging load in cold radial forging process, Int J Adv Manuf Technol 33 (2007) 7–17.
[16] A. Ghaei, A. Karimi Taheri, M.R. Movahhedy: A new upper bound solution for analysis of the radial forging process, International Journal of Mechanical Sciences 48 (2006) 1264–1272.
[17] E. Moumi, S. Ishkina, B. Kuhfuss, T. Hochrainer, A. Struss, M. Hunkel: 2D-simulation of Material Flow During Infeed Rotary Swaging Using Finite Element Method, Procedia Engineering 81 (2014) 2342–2347.
[18] F. Heislitz: Kraftbedarf beim Kaltrundkneten: Vorhaben Nr. 224. Vergleichende Untersuchungen des Kraftbedarfs beim Kaltrundkneten mit unterschiedlichen Maschinenkonzepten. Abschlussbericht, Forschungshefte. Forschungskuratorium Maschinenbau e. V. (FKM) (2000).
[19] F. Dörr, M. Liewald, J. Ostrowski, M. Werner: Wässrige Kühlschmierstoffe beim Rundkneten: Untersuchungen zur Oberflächenqualität, Spülwirkung und Prozesstemperatur neuer Kühlschmierstoffe, wt Werkstattstechnik online 103 (2013).
[20] M. Herrmann, C. Schenck, H. Leopold, B. Kuhfuss: Material improvement of mild steel S355J2C by hot rotary swaging, Procedia Manufacturing (2020).
[21] F. Böhmermann, H. Hasselbruch, M. Herrmann, O. Riemer, A. Mehner, H.-W. Zoch, B. Kuhfuß: Trockenrundkneten: Funktionalisierte Werkzeugoberflächen für eine schmierstofffreie Prozessauslegung, wt Werkstattstechnik online 105 (2015).
[22] M. Sanjari, A. Karimi Taheri, A. Ghaei: Prediction of neutral plane and effects of the process parameters in radial forging using an upper bound solution, Journal of Materials Processing Technology 186 (2007) 147–153.
[23] Y. Wu, X. Dong, Q. Yu: An upper bound solution of axial metal flow in cold radial forging process of rods, International Journal of Mechanical Sciences 85 (2014) 120–129.
[24] A. Ghaei, M.R. Movahhedy, A.K. Taheri: Study of the effects of die geometry on deformation in the radial forging process, Journal of Materials Processing Technology 170 (2005) 156–163.
[25] A. Ghaei, M.R. Movahhedy, A. Karimi Taheri: Study of the effects of die shape geometry on deformation in radial forging process without mandrel, AMME, Conference Proceedings (2003) 1112–1114.
[26] A. Ghaei, M.R. Movahhedy: Die design for the radial forging process using 3D FEM, Journal of Materials Processing Technology 182 (2007) 534–539.
[27] M. Afrasiab, H. Afrasiab, M.R. Movahhedy, G. Faraji: Design of the Die Profile for the Incremental Radial Forging Process, Transactions of Mechanical Engineering 39 (2015) 89–100.
[28] A. Ghaei, M.R. Movahhedy, A. Karimi Taheri: Finite element modelling simulation of radial forging of tubes without mandrel, Materials & Design 29 (2008) 867–872.
[29] O. Pantalé, B. Gueye: Influence of the Constitutive Flow Law in FEM Simulation of the Radial Forging Process, Journal of Engineering 2013 (2013) 1–8.
[30] L. Rong, Z. Nie, T. Zuo: FEA modeling of effect of axial feeding velocity on strain field of rotary swaging process of pure magnesium, Transactions of Nonferrous Metals Society of China 16 (2006) 1015–1020.
[31] A. Brosius, A. Mousavi: Lubricant free deep drawing process by macro structured tools, CIRP Annals 65 (2016) 253–256.

[32] F. Böhmermann, O. Riemer: Tribological performance of textured micro forming dies, Dry metal forming open access journal fast manuscript track (2016) 67–71.
[33] E. Brinksmeier, O. Riemer, S. Twardy: Tribological behavior of microstructured surfaces for micro forming tools, International Journal of Machine Tools and Manufacture 50 (2010) 425–430.
[34] N.P. Suh, N. Saka: Surface Engineering, CIRP Annals 36 (1987) 403–408.
[35] B. Schultrich, V. Weihnacht: Tribologisches Verhalten von harten und superharten Kohlenstoffschichten, VIP 20 (2008) 12–17.
[36] B. Podgornik, S. Hogmark, O. Sandberg: Influence of surface roughness and coating type on the galling properties of coated forming tool steel, Surface and Coatings Technology 184 (2004) 338–348.
[37] P. Carlsson, M. Olsson: PVD coatings for sheet metal forming processes—a tribological evaluation, Surface and Coatings Technology 200 (2006) 4654–4663.
[38] A. Ghiotti, S. Bruschi: Tribological behaviour of DLC coatings for sheet metal forming tools, Wear 271 (2011) 2454–2458.
[39] A. Erdemir, O.L. Eryilmaz, G. Fenske: Synthesis of diamondlike carbon films with superlow friction and wear properties, Journal of Vacuum Science & Technology A: Vacuum, Surfaces, and Films 18 (2000) 1987–1992.
[40] J. Heinrichs, S. Jacobson: Mechanisms of Transfer of Aluminium to PVD-Coated Forming Tools, Tribology Letters 46 (2012) 299–312.
[41] T. Horiuchi, S. Yoshihara, Y. Iriyama: Dry deep drawability of A5052 aluminum alloy sheet with DLC-coating, Wear 286-287 (2012) 79–83.
[42] T. Abraham, G. Bräuer, F. Kretz, P. Groche: Evaluation of silicon-modified DLC coatings in dry sliding contact against aluminum EN AW-5083, Dry Metal Forming OAJ FMT (2016) 11–17.
[43] H. Hetzner: Systematische Entwicklung amorpher Kohlenstoffschichten unter Berücksichtigung der Anforderungen der Blechmassivumformung, Dissertation (2014).
[44] M. Murakawa, M. Jin, M. Hayashi: Study on semidry/dry wire drawing using DLC coated dies, Surface and Coatings Technology 177-178 (2004) 631–637.
[45] X. Tan: Comparisons of friction models in bulk metal forming, Tribology International 35 (2002) 385–393.
[46] E. Doege: Fließkurvenatlas metallischer Werkstoffe: mit Fließkurven für 73 Werkstoffe und einer grundlegenden Einführung, Hanser Verlag München Wien, 1986.
[47] M. Herrmann: Schmierstofffreies Rundkneten / Trockenrundkneten, Bremen, 2019.
[48] Simula: Abaqus User's Guide, 2018.
[49] M. Herrmann, F. Böhmermann, H. Hasselbruch, B. Kuhfuss, O. Riemer, A. Mehner, H.-W. Zoch: Forming without Lubricant – Functionalized Tool Surfaces for Dry Forming Applications, Procedia Manufacturing 8 (2017) 533–540.
[50] H. Hasselbruch, M. Herrmann, A. Mehner, H.-W. Zoch, B. Kuhfuss: Development, characterization and testing of tungsten doped DLC coatings for dry rotary swaging, MATEC Web of Conferences 21 (2015) 8012.
[51] P. Bharathy, Q. Yang, M.S.R.N. Kiran, J. Rha, D. Nataraj, D. Mangalaraj: Reactive biased target ion beam deposited W–DLC nanocomposite thin films — Microstructure and its mechanical properties, Diamond and Related Materials 23 (2012) 34–43.
[52] C. Schmid, H. Hetzner, S. Tremmel, F. Hilpert, K. Durst: Tailored Mechanical Properties and Residual Stresses of a-C:H:W Coatings, Advanced Materials Research 996 (2014) 14–21.
[53] X. Chen, Z. Peng, Z. Fu, S. Wu, W. Yue, C. Wang: Microstructural, mechanical and tribological properties of tungsten-gradually doped diamond-like carbon films with functionally graded interlayers, Surface and Coatings Technology 205 (2011) 3631–3638.
[54] A. Czyzniewski: Optimising deposition parameters of W-DLC coatings for tool materials of high speed steel and cemented carbide, Vacuum 86 (2012) 2140–2147.
[55] M. Herrmann, B. Kuhfuss, C. Schenck: Dry Rotary Swaging - Tube Forming, Key engineering materials KEM 651/653 (2015) (2015) 1042–1047.
[56] A. Almohallami, M. Arghavani, F. Böhmermann, H. Freiße, M. Herrmann, A. Mousavi, S. Schöler, P. Scholz, J. Tenner, M. Teller, G. Umlauf, D. Wulff, D. Yilkiran, H.J. Maier: How dry is dry? - A critical analysis of surface conditions used in dry metal forming, Dry Metal Forming OAJ FMT 3 (2017) 90–94.
[57] F. Böhmermann, M. Herrmann, O. Riemer, B. Kuhfuß: Abrasive Particle Generation in Dry Rotary Swaging, Dry Metal Forming Open Access Journal (2017) 1–6.
[58] F. Böhmermann, M. Herrmann, O. Riemer, B. Kuhfuß: Reducing Abrasive Particle Generation in Dry Rotary Swaging by Utilizing DLC Hard Coated Dies, MATEC Web of Conferences (2018) 14011.
[59] M. Herrmann, Y. Liu, C. Schenck, B. Kuhfuss, I. Ohlsen: Evolution of heat in dry rotary swaging, AIP Conference Proceedings 1896 (2017) 80018.
[60] F. Böhmermann, H. Hasselbruch, M. Herrmann, O. Riemer, A. Mehner, H.-W. Zoch, B. Kuhfuss: Dry rotary swaging–approaches for lubricant free process design, Int. J. of Precis. Eng. and Manuf.-Green Tech. 2 (2015) 325–331.
[61] M. Herrmann, C. Schenck, B. Kuhfuss: Dry Rotary Swaging with Structured Tools, Procedia CIRP 40 (2016) 653–658.
[62] H. Hasselbruch, M. Herrmann, A. Mehner, B. Kuhfuss, H.-W. Zoch: Incremental dry forging - Interaction of W-DLC Coatings and Surface Structures for Rotary Swaging Tools, Procedia Manufacturing 8 (2017) 541–548.
[63] M. Herrmann, C. Schenck, B. Kuhfuss: FEM simulation of infeed rotary swaging with structured tools, MATEC Web of Conferences 21 (2015) 12003.
[64] M. Herrmann, C. Schenck, B. Kuhfuss: Graded Structured Tools for Dry Rotary Swaging, Dry Metal Forming Open Access Journal (2018) 18–24.
[65] Y. Liu, M. Herrmann, C. Schenck, B. Kuhfuss: Plastic deformation history in infeed rotary swaging process, AIP Conference Proceedings (2017) 80013.
[66] R. Ebrahimi, A. Najafizadeh: A new method for evaluation of friction in bulk metal forming, Journal of Materials Processing Technology 152 (2004) 136–143.
[67] F. Böhmermann, O. Riemer: Development and application of a test rig for tribological investigations under impact loads, CIRP Journal of Manufacturing Science and Technology 19 (2017) 129–137.
[68] H. Hasselbruch, B. Lenz, A. Mehner: Statistical approach of a semi-automatic method for determining the Rockwell substrate adhesion of a-C:H(:W) coat-ings by using a combination convolutional neural networks and image analysis, Surface and Coatings Technology (2020).
[69] M. Zawischa, S. Makowski, N. Schwarzer, V. Weihnacht: Scratch resistance of superhard carbon coatings – A new approach to failure and adhesion evaluation, Surface and Coatings Technology 308 (2016) 341–348.
[70] H. Hasselbruch, B. Lenz, H. Großmann, A. Mehner: Correlation between a semi-automatic incremental image analysis and acoustic emissions (AE) for scratch testing of thin a-C:H:W caotings, Surface and Coatings Technology (2020).
[71] G. Stoney: The tension of metallic films deposited by electrolysis, Proceedings of the Royal Society of London. A. Mathematical and Physical Sciences 82 (1909) 172–175.
[72] A. Brenner, S. Senderoff: Calculation of stress in electrodeposits from the curvature of a plated strip, Journal of Research of the National Bureau of Standards 42 (1949) 105.
[73] M. Benabdi, A.A. Roche: Mechanical properties of thin and thick coatings applied to various substrates. Part I. An elastic analysis of residual stresses within coating materials, Journal of Adhesion Science and Technology 11 (1997) 281–299.
[74] H.-J. Bargel, G. Schulze: Werkstoffkunde, Springer Berlin Heidelberg, Berlin, Heidelberg, 2008.

[75] S.-J. Cho, K.-R. Lee, K. Yong Eun, J. Hee Hahn, D.-H. Ko: Determination of elastic modulus and Poisson's ratio of diamond-like carbon films, Thin Solid Films 341 (1999) 207–210.
[76] K.-D. Bouzakis, G. Maliaris, S. Makrimallakis: Strain rate effect on the fatigue failure of thin PVD coatings: An investigation by a novel impact tester with adjustable repetitive force, International Journal of Fatigue 44 (2012) 89–97.
[77] H. Hasselbruch, A. Mehner, H.-W. Zoch: Einfluss der Plasmanitrierparameter und anschließenden Oberflächenveredelung auf die Haftfestigkeit von Wolfram dotierten PVD-a-C:H-Schichtsystemen, Proceedings of 58th Tribologie-Fachtagung (2017) 59/1-59/11.
[78] H. Hasselbruch, A. Mehner, H.-W. Zoch: Influence of plasma nitriding parameters and subsequent surface finishing on the adhesion strength of tungsten doped PVD a-C:H coatings, Proceedings of 13th International Conference of THE"A" Coatings (2017) 1–10.
[79] M. Herrmann, H. Hasselbruch, F. Böhmermann, B. Kuhfuß, H.-W. Zoch, A. Mehner, O. Riemer: Potentials of dry rotary swaging, Dry metal forming open access journal fast manuscript track (2015) 63–71.
[80] H. Hasselbruch, M. Herrmann, J. Heidhoff, H.-W. Zoch, B. Kuhfuss, O. Riemer, A. Mehner: Strukturierte und DUPLEX behandelte Werkzeuge für die Trockenbearbeitung beim Rundkneten, Dry Metal Forming Open Access Journal (2019) 31–38.
[81] F. Böhmermann, M. Herrmann, O. Riemer, B. Kuhfuss: Reducing Abrasive Particle Generation in Dry Rotary Swaging by Utilizing DLC Hard Coated Dies, MATEC Web of Conferences 190 (2018) 14011.
[82] A. Ovcharenko, G. Halperin, I. Etsion: In situ and real-time optical investigation of junction growth in spherical elastic–plastic contact, Wear 264 (2008) 1043–1050.
[83] K.-D. Bouzakis, A. Siganos, T. Leyendecker, G. Erkens: Thin hard coatings fracture propagation during the impact test, Thin Solid Films 460 (2004) 181–189.